Atmos. Chem. Phys., 17, 8725–8738, 2017
https://doi.org/10.5194/acp-17-8725-2017

Atmospheric Chemistry and Physics
Open Access
EGU

Glyoxal yield from isoprene oxidation and relation to formaldehyde: chemical mechanism, constraints from SENEX aircraft observations, and interpretation of OMI satellite data

Christopher Chan Miller[1], Daniel J. Jacob[1,2], Eloise A. Marais[1], Karen Yu[2], Katherine R. Travis[2], Patrick S. Kim[1], Jenny A. Fisher[3], Lei Zhu[2], Glenn M. Wolfe[4,5], Thomas F. Hanisco[4], Frank N. Keutsch[2,6], Jennifer Kaiser[7,a], Kyung-Eun Min[8,9,b], Steven S. Brown[9,10], Rebecca A. Washenfelder[8,9], Gonzalo González Abad[11], and Kelly Chance[11]

[1]Department of Earth and Planetary Sciences, Harvard University, Cambridge, MA, USA
[2]School of Engineering and Applied Sciences, Harvard University, Cambridge, MA, USA
[3]School of Chemistry and School of Earth and Environmental Sciences, University of Wollongong, Wollongong, NSW, Australia
[4]Atmospheric Chemistry and Dynamics Lab, NASA Goddard Space Flight Center, Greenbelt, MD, USA
[5]Joint Center for Earth Systems Technology, University of Maryland Baltimore County, Baltimore, MD, USA
[6]Department of Chemistry and Chemical Biology, Harvard University, Cambridge, MA, USA
[7]Department of Chemistry, University of Wisconsin Madison, Madison, WI, USA
[8]Cooperative Institute for Research in Environmental Sciences, University of Colorado Boulder, Boulder, CO, USA
[9]Chemical Sciences Division, NOAA Earth System Research Laboratory, Boulder, CO, USA
[10]Department of Chemistry and Biochemistry, University of Colorado, Boulder, CO, USA
[11]Harvard-Smithsonian Center for Astrophysics, Cambridge, MA, USA
[a]now at: School of Engineering and Applied Sciences, Harvard University, Cambridge, MA, USA
[b]now at: School of Earth Sciences and Environmental Engineering, Gwangju Institute of Science and Technology, Gwangju, South Korea

Correspondence to: Daniel J. Jacob (djacob@fas.harvard.edu)

Received: 23 November 2016 – Discussion started: 29 November 2016
Revised: 5 June 2017 – Accepted: 7 June 2017 – Published: 18 July 2017

Abstract. Glyoxal (CHOCHO) is produced in the atmosphere by the oxidation of volatile organic compounds (VOCs). Like formaldehyde (HCHO), another VOC oxidation product, it is measurable from space by solar backscatter. Isoprene emitted by vegetation is the dominant source of CHOCHO and HCHO in most of the world. We use aircraft observations of CHOCHO and HCHO from the SENEX campaign over the southeast US in summer 2013 to better understand the CHOCHO time-dependent yield from isoprene oxidation, its dependence on nitrogen oxides ($NO_x \equiv NO + NO_2$), the behavior of the CHOCHO–HCHO relationship, the quality of OMI CHOCHO satellite observations, and the implications for using CHOCHO observations from space as constraints on isoprene emissions. We simulate the SENEX and OMI observations with the Goddard Earth Observing System chemical transport model (GEOS-Chem) featuring a new chemical mechanism for CHOCHO formation from isoprene. The mechanism includes prompt CHOCHO formation under low-NO_x conditions following the isomerization of the isoprene peroxy radical ($ISOPO_2$). The SENEX observations provide support for this prompt CHOCHO formation pathway, and are generally consistent with the GEOS-Chem mechanism. Boundary layer CHOCHO and HCHO are strongly correlated in the observations and the model, with some departure under low-NO_x conditions due to prompt CHOCHO formation. SENEX vertical profiles indicate a free-tropospheric CHOCHO background that is absent from the model. The OMI CHOCHO data provide some support for this free-tropospheric background and show southeast US enhancements consistent with the iso-

prene source but a factor of 2 too low. Part of this OMI bias is due to excessive surface reflectivities assumed in the retrieval. The OMI CHOCHO and HCHO seasonal data over the southeast US are tightly correlated and provide redundant proxies of isoprene emissions. Higher temporal resolution in future geostationary satellite observations may enable detection of the prompt CHOCHO production under low-NO_x conditions apparent in the SENEX data.

1 Introduction

Glyoxal (CHOCHO) and formaldehyde (HCHO) are short-lived products of the atmospheric oxidation of volatile organic compounds (VOCs). Both are detectable from space by solar backscatter (Chance et al., 2000; Wittrock et al., 2006). Isoprene emitted by terrestrial vegetation accounts for about a third of the global source of non-methane VOCs (NMVOCs Guenther et al., 2012) and drives large enhancements of CHOCHO and HCHO in the continental boundary layer (Palmer et al., 2003; Fu et al., 2008). Satellite observations of HCHO have been widely used as a proxy to estimate isoprene emissions (Abbot et al., 2003; Palmer et al., 2006; Millet et al., 2008; Curci et al., 2010; Barkley et al., 2013), but there are uncertainties related to the HCHO yield from isoprene oxidation (Marais et al., 2012) and the role of other NMVOCs as HCHO precursors (Fu et al., 2007). CHOCHO observations from space could provide a complementary constraint (Vrekoussis et al., 2009, 2010; Alvarado et al., 2014; Chan Miller et al., 2014). Here we use CHOCHO and HCHO aircraft observations over the southeast US from the summer 2013 Southeast Nexus (SENEX) campaign (Warneke et al., 2016), interpreted with the Goddard Earth Observing System chemical transport model (GEOS-Chem), to test understanding of the CHOCHO yield from isoprene oxidation, its dependence on nitrogen oxide radicals ($NO_x \equiv NO + NO_2$), and the combined value of the CHOCHO–HCHO pair measured from space to constrain isoprene emissions and chemistry.

Isoprene impacts air quality and climate as a precursor to ozone (Geng et al., 2011) and secondary organic aerosol (SOA Carlton et al., 2009), and also affects concentrations of hydrogen oxide radicals ($HO_x \equiv OH + HO_2$; Peeters and Muller, 2010) and NO_x (Mao et al., 2013; Fisher et al., 2016). Atmospheric oxidation of isoprene by OH takes place on a timescale of less than an hour to produce organic peroxy radicals ($ISOPO_2$). Reaction of $ISOPO_2$ with NO drives production of ozone and of organic nitrates that serve as a reservoir for NO_x (Browne and Cohen, 2012). At lower NO_x levels, $ISOPO_2$ reacts dominantly with HO_2 to produce isoprene epoxydiols (IEPOX) via isoprene peroxides (ISOPOOH; Paulot et al., 2009b), and from there isoprene SOA (Marais et al., 2016). $ISOPO_2$ can also isomerize to generate HO_x radicals (Peeters et al., 2009, 2014; Crounse et al., 2011).

The fate of $ISOPO_2$ determines the production rates and overall yields of CHOCHO and HCHO. Several studies have provided insight on the time- and NO_x-dependent yield of HCHO (Palmer et al., 2003; Marais et al., 2012; Wolfe et al., 2016). Under high-NO_x conditions, HCHO production is sufficiently prompt that observed HCHO columns can be locally related to isoprene emission rates (Palmer et al., 2006). This assumption is the basis of many studies that have used satellite HCHO observations to constrain isoprene emissions (Palmer et al., 2006; Fu et al., 2007; Millet et al., 2008; Curci et al., 2010). HCHO production is much slower under low-NO_x conditions, spatially "smearing" the local relationship between isoprene emissions and HCHO columns. This has been addressed by using concurrent satellite data for NO_2 columns to correct the isoprene–HCHO relationship (Marais et al., 2012) or by using adjoint-based inverse modeling to relate HCHO columns to isoprene emissions including the effect of transport (Fortems-Cheiney et al., 2012).

Isoprene is estimated to account for about $\sim 50\,\%$ of global CHOCHO production (Fu et al., 2008), but there is large uncertainty regarding the yield of CHOCHO from isoprene oxidation. Open fires and aromatic VOCs can also be major sources of CHOCHO (Volkamer et al., 2001; Fu et al., 2008; Chan Miller et al., 2016). Several studies have used the measured CHOCHO–HCHO concentration ratio $R_{GF} = [CHOCHO]/[HCHO]$ as an indicator of the dominant VOC precursors. Vrekoussis et al. (2010) found higher R_{GF} values (> 0.04) from GOME-2 satellite observations in regions where biogenic VOCs are dominant, and lower values where anthropogenic VOCs are dominant. However, the opposite behavior is observed in ground-based studies (Di-Gangi et al., 2012). Our recent CHOCHO retrieval from the OMI satellite instrument (Chan Miller et al., 2014) is in better agreement with surface observations of CHOCHO and R_{GF} (Kaiser et al., 2015) compared to those from GOME-2 (Vrekoussis et al., 2010) and SCIAMACHY (Wittrock et al., 2006) as a result of improved background corrections and removal of NO_2 interferences. There remains the question of how observed CHOCHO–HCHO relationships are to be interpreted.

The Southeast Nexus (SENEX) aircraft campaign was conducted over the southeast US in June–July 2013. The aircraft had a detailed chemical payload including in situ CHOCHO (Min et al., 2016) and HCHO (Cazorla et al., 2015). Thirteen daytime flights were conducted over the campaign with extensive boundary layer coverage. Li et al. (2016) recently used the SENEX observations to evaluate CHOCHO formation from isoprene in the AM3 chemical transport model (CTM). They found that the AM3 mechanism had closer agreement with observations than the explicit Master Chemical Mechanism v3.3.1 (MCMv3.3.1; Jenkin et al., 2015), and suggested that CHOCHO yields from isoprene epoxydiols are underestimated in MCMv3.3.1. Here

we take a more rigorous look at potential missing pathways in MCMv3.3.1. In doing so, we present an improved chemical mechanism for CHOCHO formation from isoprene for the GEOS-Chem CTM, and evaluate it against the SENEX observations, including the time and NO_x dependence of the CHOCHO yield from isoprene. We discuss the implications of the new mechanism for the interpretation of satellite observations, and present a first validation of the CHOCHO retrieval from the OMI satellite instrument (Chan Miller et al., 2014).

2 GEOS-Chem model description

2.1 General description

We use the same version of GEOS-Chem v9.2 (http://www.geos-chem.org) that has been used previously to interpret chemical observations from the NASA SEAC^{4}RS aircraft campaign conducted in the same southeast US region in August–September 2013 (Travis et al., 2016; Fisher et al., 2016). The model is driven by assimilated meteorological data with $0.25° \times 0.3125°$ horizontal resolution from the Goddard Earth Observing System (GEOS-FP) reanalysis product (Molod et al., 2012). The native $0.25° \times 0.3125°$ resolution is retained in GEOS-Chem over the North American domain (130–60° W, 9.75–60° N), nested within a global simulation at $2° \times 2.5°$ resolution (Kim et al., 2015). Isoprene chemistry in GEOS-Chem v9.2 is as described by Mao et al. (2013), but the SEAC^{4}RS simulation includes a number of updates described by Travis et al. (2016) and Fisher et al. (2016). The simulation presented here includes further modifications relevant to CHOCHO, listed in the Supplement (Table S1) and summarized below. Evaluation of the model with SEAC^{4}RS observations has been presented by Kim et al. (2015) for aerosols, Travis et al. (2016) for ozone and NO_x, Fisher et al. (2016) for organic nitrates, Marais et al. (2016) for isoprene SOA, and Zhu et al. (2016) for HCHO including satellite validation.

Isoprene emissions in the model are from MEGANv2.1 (Guenther et al., 2012) with a 15 % reduction (Kim et al., 2015), and NO_x emissions are as described by Travis et al. (2016) including a 50 % decrease in the anthropogenic source relative to the 2011 National Emission Inventory of the US Environmental Protection Agency. Yu et al. (2016) pointed out that isoprene and NO_x emissions in the southeast US are spatially segregated and show that the $0.25° \times 0.3125°$ resolution of GEOS-Chem is adequate for separating the populations of high- and low-NO_x conditions for isoprene oxidation.

2.2 CHOCHO formation from isoprene and loss

Figure 1 shows the CHOCHO formation pathways from isoprene oxidation by OH (the main isoprene sink) as implemented in this work. Oxidation is initiated by OH addition to the terminal carbons of the isoprene double bonds (positions 1 and 4, Fig. 1). Isoprene peroxy radicals ($ISOPO_2$) are formed by O_2 addition to the carbon either in β or δ to the hydroxyl carbon. $ISOPO_2$ reacts with NO and HO_2, and also isomerizes. Together these pathways represent 92 % of $ISOPO_2$ loss, with the remainder due to reactions with organic peroxy radicals.

Under high-NO_x conditions, CHOCHO is produced promptly via products of the δ isomers (HC5, DIBOO; Paulot et al., 2009a; Galloway et al., 2011). CHOCHO production via the β isomers is slower, due to the intermediary production of methylvinylketone (MVK) followed by glycolaldehyde (GLYC). GEOS-Chem originally had a fixed δ vs. β branching ratio of 24 % for the reaction of $ISOPO_2 + NO$, based on the chamber experiments of Paulot et al. (2009a). However recent work has shown that O_2 addition to the isoprene–OH adducts is reversible (pink pathway, Fig. 1), allowing interconversion between β and δ $ISOPO_2$ isomers (Peeters et al., 2009, 2014; Crounse et al., 2011). Isomers of β are heavily favored at equilibrium, accounting for ~ 95 % of $ISOPO_2$ (Peeters et al., 2014). The experimental conditions in Paulot et al. (2009a) used high NO_x concentrations (~ 500 ppbv). This implies short $ISOPO_2$ lifetimes, and thus may not reflect the degree of isomer interconversion seen at ambient oxidant levels. Here we adopt a δ-$ISOPO_2$ branching ratio of 10 %, following Fisher et al. (2016), to match SEAC^{4}RS observations of organic nitrates produced through the δ-$ISOPO_2 + NO$ pathway.

CHOCHO forms under low-NO_x conditions through isoprene epoxydiols (IEPOX) and through the $ISOPO_2$ isomerization pathway. IEPOX forms as a second-generation non-radical product of isoprene oxidation via ISOPOOH, and thus represents a slow CHOCHO formation pathway. IEPOX isomer fractions in GEOS-Chem are based on equilibrium δ/β $ISOPO_2$ branching ratios (Bates et al., 2014; Travis et al., 2016). At low NO_x levels the $ISOPO_2$ lifetime is sufficiently long for equilibrium to be reached (Peeters et al., 2014). $ISOPO_2$ isomerization in the previous GEOS-Chem mechanism of Travis et al. (2016) produced solely hydroperoxyaldehydes (HPALDs), but here we also include the formation of dihydroperoxy α-formyl peroxy radicals (di-HPCARPs; Peeters et al., 2014) following MCMv3.3.1. di-HPCARPs in MCMv3.3.1 have a low CHOCHO yield, but here we introduce a (1,5)H-shift isomerization of di-HPCARPs that could be competitive with the (1,4)H-shift isomerization due to the presence of the terminal-peroxide functional group (Crounse et al., 2013). The resulting di-hydroperoxide dicarbonyl compound (DHDC) product quickly photolyzes to produce CHOCHO, analogous to the mechanisms proposed for HPALDs (Peeters et al., 2014) and carbonyl nitrates (Müller et al., 2014). As shown below, we find that this pathway can explain SENEX observations of prompt CHOCHO production under low-NO_x conditions.

The mechanism presented here differs substantially from the AM3 mechanism previously used by Li et al. (2016)

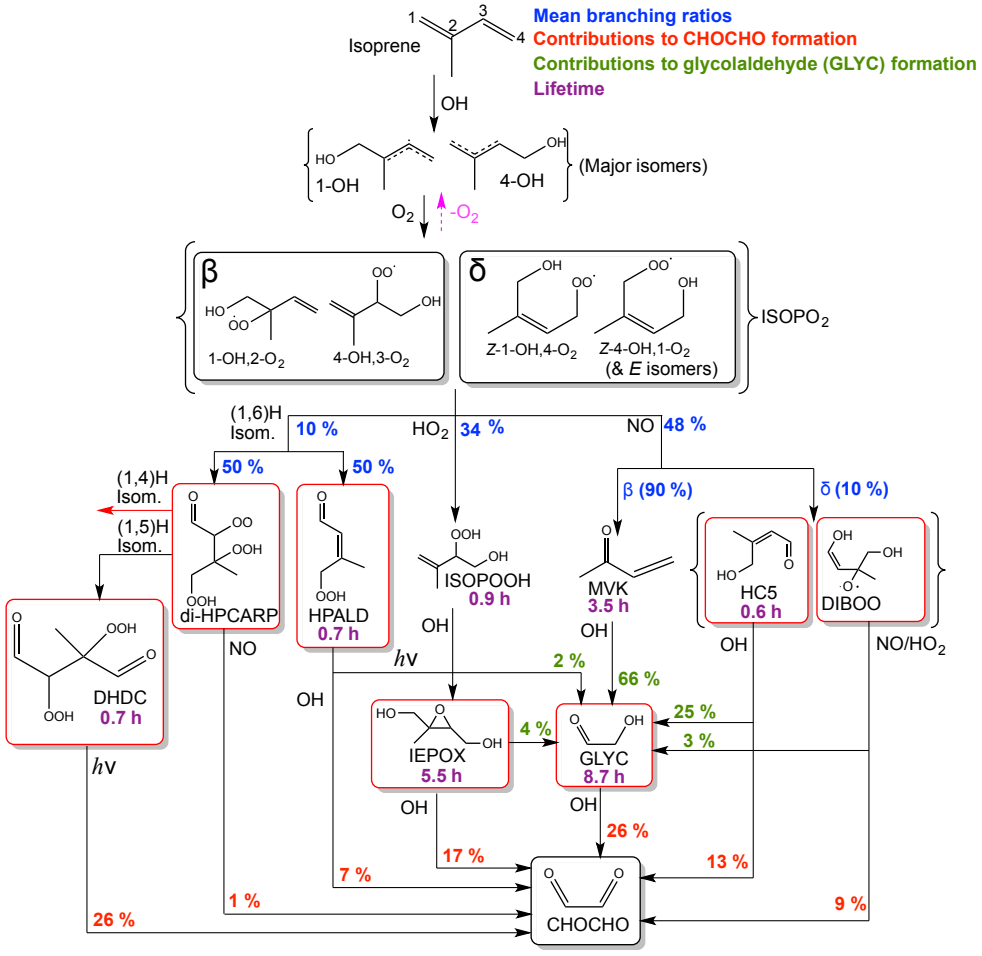

Figure 1. Pathways for glyoxal (CHOCHO) formation from isoprene oxidation in GEOS-Chem as implemented in this work. Only species relevant to CHOCHO formation are shown. Branching ratios, species lifetimes, and contributions to glyoxal and glycolaldehyde (GLYC) formation from each boxed species are mean values over the southeast US (96.25–73.75° W, 29–41° N) during the SENEX campaign (1 June–10 July 2013). Species lifetimes are shown for an OH concentration of 4×10^6 molecules cm^{-3}.

to analyze the SENEX observations. Li et al. (2016) tested branching ratios of 22 and 0 % for δ-ISOPO$_2$ + NO, with the latter intended to reflect ISOPO$_2$ isomer interconversion. The 10 % branching ratio in this study is constrained by SEAC^{4}RS organic nitrate observations (Fisher et al., 2016). Li et al. (2016) report a CHOCHO yield from GLYC oxidation (Sect. S1 in the Supplement), which is mainly due to a lower CHOCHO yield from GLYC + OH (13 % vs. 20 %). Their yield of CHOCHO from IEPOX is 28 %, much higher than can be accommodated by yields of hydroxyacetone derived from IEPOX oxidation chamber experiments (Bates et al., 2014) (the expected coproduct of CHOCHO via this pathway, Sect. S2). Following Travis et al. (2016), we set the CHOCHO yield from IEPOX to the corresponding hydroxyacetone yields reported by Bates et al. (2014) (8.5 % via HO$_2$ and 8.8 % via NO). Finally AM3 assumes 25 % CHOCHO yield from HPALD photolysis following Stavrakou et al. (2010), which has been used in many past studies (Mao et al., 2013; Marais et al., 2016). However HPALD photolysis is not expected to yield CHOCHO (Sect. S3). The CHOCHO formation pathway via DHDC proposed here can be justified from existing literature (Sect. S3). Inclusion of DHDC increases the yield of CHOCHO via ISOPO$_2$ isomerization by 18 %, which is comparable to the AM3 yield.

Li et al. (2016) found that CHOCHO concentrations are sensitive to aerosol reactive uptake. Our standard model simulation does not include this uptake, but we conducted a sensitivity simulation with a reactive uptake coefficient $\gamma = 2 \times 10^{-3}$ from Li et al. (2016). We find that CHOCHO concentrations decrease by only 10 % on average (Sect. S4) because competing CHOCHO sinks from reaction with OH and photolysis are fast.

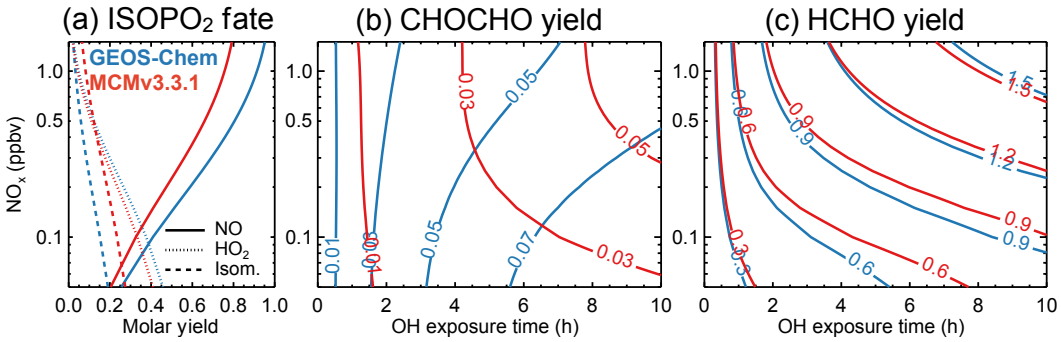

Figure 2. Cumulative time- and NO_x-dependent molar yields of CHOCHO and HCHO from isoprene oxidation in the GEOS-Chem and MCM3.3.1 chemical mechanisms. Results are from box model simulations with fixed NO_x concentrations as described in the text, and are presented as functions of the imposed NO_x concentration (vertical axis). Panel **(a)** shows the isoprene peroxy radical ($ISOPO_2$) branching ratios for reaction with NO, HO_2, and isomerization. Panels **(b, c)** show the time-dependent cumulative yields of CHOCHO and HCHO, where time is normalized by OH exposure (Eq. 1). "OH exposure time" is equivalent to time for a constant $[OH] = 4 \times 10^6$ molecules cm^{-3}.

2.3 Time- and NO_x-dependent CHOCHO and HCHO yields from isoprene

Understanding the time- and NO_x-dependent yields of CHOCHO and HCHO from isoprene oxidation is critical for interpreting observed CHOCHO and HCHO columns from space in terms of isoprene emissions. Here we examine time-dependent CHOCHO and HCHO molar yields in the GEOS-Chem and MCMv3.3.1 chemical mechanisms using the Dynamically Simple Model of Atmospheric Chemical Complexity (DSMACC) box model (Emmerson and Evans, 2009). Simulations are initiated at 09:00 LT with 1 ppbv isoprene, 40 ppbv O_3, and 100 ppbv CO. NO_x concentrations are held at fixed values. Photolysis rates are calculated for clear sky with the TUV radiative transfer model (Madronich, 1987). To correct for differences in time-dependent yields associated with differences in OH concentrations, we reference GEOS-Chem and MCMv3.3.1 results to a common "OH exposure time" variable (t_{OH}):

$$t_{OH} = \frac{1}{[OH]_{ref}} \int_0^t [OH](t')dt'. \quad (1)$$

Here $[OH](t)$ is the OH concentration simulated in the box model, and $[OH]_{ref} = 4 \times 10^6$ molecules cm^{-3} is a reference OH concentration representative of summer daytime conditions over the southeast US (Wolfe et al., 2016). For a fixed $[OH] = 4 \times 10^6$ molecules cm^{-3}, t_{OH} represents the actual time.

Figure 2 shows the time- and NO_x-dependent cumulative molar yields of CHOCHO and HCHO in GEOS-Chem and MCMv3.3.1. The branching ratio of $ISOPO_2$ as a function of NO_x is also shown. The time-dependent HCHO yields in both mechanisms are similar under high-NO_x conditions. Additional confidence in the HCHO yield under these conditions is offered by the ability of GEOS-Chem to reproduce the observed correlation between HCHO and isoprene organic nitrates (Mao et al., 2013; Fisher et al., 2016). The HCHO yield is lower under low-NO_x conditions in both mechanisms, and overall the difference between them is minor.

There is far more disagreement between the two mechanisms for CHOCHO yields. Under high-NO_x conditions, GEOS-Chem produces CHOCHO rapidly in the first 2 h due to its higher δ-$ISOPO_2$+NO branching ratio (10 % in GEOS-Chem vs. 3.4 % in MCMv3.3.1). This is compensated at longer OH exposure times by higher GLYC yields from isoprene in MCMv3.3.1. GEOS-Chem produces higher ultimate yields of CHOCHO under low-NO_x conditions mainly due to DHDC formation and subsequent photolysis, neither of which are included in MCMv3.3.1. The NO_x-dependence of the CHOCHO yield in MCMv3.3.1 is similar to that of HCHO, implying that CHOCHO and HCHO observations would provide redundant information on isoprene emissions. The SENEX observations indicate that CHOCHO yields under low-NO_x conditions are too low in MCMv3.3.1, as discussed below. In GEOS-Chem, by contrast, the CHOCHO and HCHO yields show opposite dependences on NO_x, implying that they could provide complementary information on isoprene emissions.

3 Constraints from SENEX observations

Figure 3 shows the observed and simulated median vertical profiles of CHOCHO, HCHO, and NO_x concentrations along the SENEX flight tracks. Figure 4 shows maps of concentrations below 1 km altitude (above ground level) taken as the mixed layer. Here and elsewhere we only include daytime observations (10:00–17:00 LT) and exclude targeted sampling of biomass burning plumes (diagnosed by acetonitrile concentrations above 200 pptv). CHOCHO, HCHO, and NO_x were measured by the Airborne Cavity Enhanced

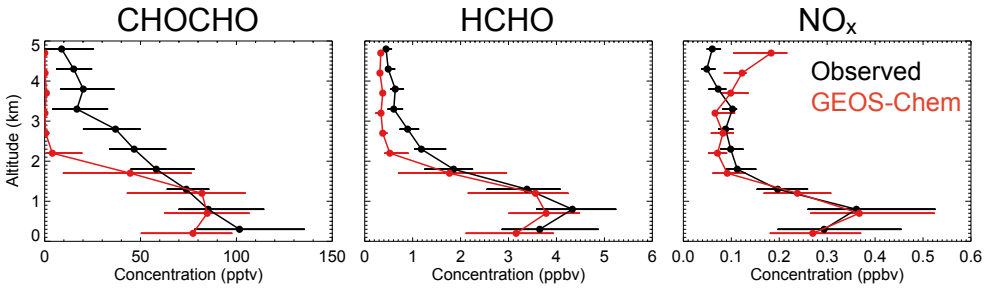

Figure 3. Median vertical profiles of CHOCHO, HCHO, and NO_x concentrations during SENEX (1 June–10 July 2013). Observed concentrations (Min et al., 2016; Cazorla et al., 2015; Pollack et al., 2010) are compared to GEOS-Chem model values sampled along the flight tracks. Horizontal bars indicate interquartile range. Altitudes are above ground level (a.g.l.).

Spectrometer (ACES; Min et al., 2016), In Situ Airborne Formaldehyde (ISAF) instrument (Cazorla et al., 2015), and the NOAA chemiluminescence instrument (Ryerson et al., 1999; Pollack et al., 2010), with stated accuracies of 6, 10, and 5 %, respectively.

Simulated median NO_x concentrations in the mixed layer are within 10 % of observations, supporting the 50 % reduction in EPA NEI NO_x emissions previously inferred from the analysis of SEAC^{4}RS observations by Travis et al. (2016), also included here (Sect. 2.1). Half of isoprene oxidation in the model under the SENEX conditions takes place by the low-NO_x pathways (Fig. 1). Simulated median CHOCHO and HCHO concentrations in the mixed layer are within 20 % of observations, but the model is too low at higher altitudes. During SENEX the mixed layer was typically capped by a neutrally stable transition layer of shallow cumulus convection which extended up to 3 km (Wagner et al., 2015), which could suggest that the model underestimates transport via this mechanism. However, the model does not underestimate other isoprene oxidation products in the transition layer, such as MVK + methacrolein (Fig. S8 in the Supplement). Another possible source of CHOCHO in the transition layer is via heterogeneous aerosol oxidation (Volkamer et al., 2015). However, specific aerosol precursors that produce CHOCHO at yields required to match the SENEX observations are currently unknown (Kaiser et al., 2015).

The CHOCHO observations in the free troposphere (> 3 km) have to be treated with caution since they are below the reported instrument precision (32 pptv, Kaiser et al., 2015). It is therefore difficult to determine whether the bias is due to a missing CHOCHO source in the model or instrument artifact. Elevated CHOCHO concentrations above the boundary layer have also been observed in previous campaigns over the southeast US (Lee et al., 1998), California (Baidar et al., 2013), and the remote Pacific (Volkamer et al., 2015). There could be a free-tropospheric source missing in the model, but it is unclear what this source could be, and correlative analysis of observed free-tropospheric CHOCHO with other species measured in SENEX offer no insight ($r < 0.3$ for all observed VOCs).

The mixed layer concentrations maps in Fig. 4 show that the model captures some of the horizontal variability in the observations. The spatial correlation for HCHO is high ($r = 0.75$) as in SEAC^{4}RS ($r = 0.64$, Zhu et al., 2016), and reflects isoprene emission patterns. Correlation for CHOCHO is also relatively strong ($r = 0.51$). Temporally averaged CHOCHO and HCHO concentrations simulated by the model for the SENEX period (background in Fig. 4) are much more uniform than those sampled along the SENEX flight tracks because of day-to-day variability in isoprene emissions, mostly driven by temperature (Zhu et al., 2016).

Figure 5 compares simulated and observed CHOCHO vs. HCHO relationships in the mixed layer, color coded by NO_x concentrations. Correlation between the two species is strong. The model better captures the observed slope (0.028 modeled vs. 0.024 observed) compared to the AM3 CTM (0.045 and 0.035 with and without CHOCHO production from δ-ISOPO$_2$ + NO, respectively; Li et al., 2016). Inclusion of aerosol uptake further reduces the bias to the observed slope (0.026, Fig. S10). On average, CHOCHO is produced more promptly in AM3 compared to GEOS-Chem, which may lead to the higher slope. In the first few hours of oxidation this is due to a higher CHOCHO yield from ISOPO$_2$ isomerization. Beyond the initial stages of isoprene oxidation, CHOCHO is produced faster in AM3 because of the increased fraction of CHOCHO produced from IEPOX over GLYC oxidation (Fig. 1).

The strong correlation between CHOCHO and HCHO might suggest that they provide redundant information for constraining isoprene emissions. However, examination of Fig. 5 indicates higher observed CHOCHO-to-HCHO ratios (R_{GF}) at low-NO_x concentrations, not captured by GEOS-Chem. Figure 6 shows the R_{GF} ratio as a function of NO_x below 1 km in the SENEX observations and as simulated by GEOS-Chem. Points are color coded by OH exposure time t_{OH} (Eq. 1), derived from PTR-MS observations of the methylvinylketone + methacrolein-to-isoprene ratio (de Gouw and Warneke, 2007) following Wolfe et al. (2016). The median and interquartile R_{GF} values binned in 250 pptv NO_x increments are also shown. The observed me-

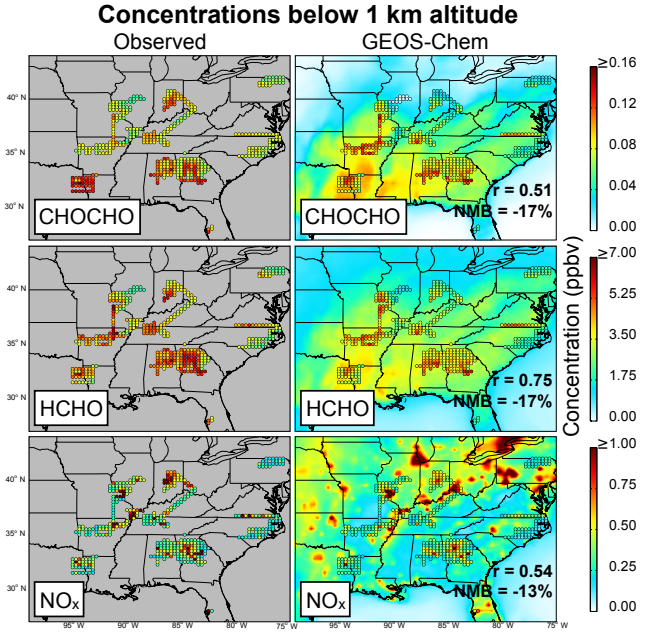

Figure 4. CHOCHO, HCHO, and NO_x concentrations below 1 km a.g.l. during SENEX (1 June–10 July 2013). The grid squares show daytime aircraft observations compared to the colocated GEOS-Chem model values on the $0.25° \times 0.3125°$ model grid. Background contours in the right panels show the average model-simulated concentrations at 13:00–14:00 LT for the SENEX period. Comparison statistics between model and observation grid squares are shown as the correlation coefficient r and the normalized mean bias (NMB). Correlation statistics for NO_2 exclude urban plumes in the observations ($[NO_x] > 4$ ppb) as these would not be resolved at the scale of the model.

dian R_{GF} values (0.02 to 0.024 mol mol^{-1}) show no significant dependence on NO_x, while GEOS-Chem shows a weak dependence.

The observations contain a subset of low-NO_x points with higher R_{GF} values (0.03–0.06). The model also produces a subset of enhanced R_{GF} values under low-NO_x conditions, although peak R_{GF} values are lower than the observations. In both cases, the enhanced R_{GF} values coincide with short OH exposure times, which are caused by OH titration by isoprene. The high R_{GF} reflects the relatively faster production of CHOCHO than HCHO in the early stage of isoprene oxidation under low-NO_x conditions as shown by Fig. 2. The presence of that population in the observations provides support for fast glyoxal production from the isomerization pathway of isoprene oxidation (Fig. 1) that is present in GEOS-Chem but not in MCMv3.3.1. The model may not capture the highest observed R_{GF} values due to uncertainties in the yield of DHDC from isoprene and its photolysis rate, both of which have been estimated based on literature proxies (Sect. S3).

Figure 6 also shows that there is a small subset of points in GEOS-Chem with RGF values less than 0.01, reflecting low CHOCHO values in the model that are not found in the observations where the concentration floor is 0.05 ppbv (Fig. 5). There may be a CHOCHO background missing from the model, possibly contributed by monoterpenes; MCMv3.3.1 predicts that the total CHOCHO yield from common monoterpenes is high (Kaiser et al., 2015), and that they produce CHOCHO over a timescale of days (Fig. S11).

4 Implications for satellite observations

Knowledge gained from SENEX enables an improved interpretation of CHOCHO and HCHO column observations from space in isoprene dominated environments. We use for this purpose June–August in 2006 and 2007 observations of CHOCHO, HCHO, and tropospheric NO_2 columns from the Ozone Monitoring Instrument (OMI). OMI was launched onboard the NASA Aura satellite in July 2004, and provides daily global coverage in sun-synchronous orbit with an equatorial crossing time of 13:40 LT. The CHOCHO data are from the Smithsonian Astrophysical Observatory (SAO) retrieval described in Chan Miller et al. (2014) and hereby referred to as OMI SAO. The HCHO and NO_2 data are from the OMI Version 3 product release (González Abad et al., 2015; Bucsela et al., 2013). Retrievals are in the 435–461 nm spectral range for CHOCHO, 328.5–356.5 nm for HCHO, and 405–465 nm for NO_2. We use 2006–2007 data because 2013 data for CHOCHO are very noisy (Fig. S12), possibly because of sensor degradation. The OMI observations are compared to a GEOS-Chem simulation covering the same period, at $2° \times 2.5°$ horizontal resolution.

Slant columns along the optical path of the backscattered solar radiation are fitted to the observed spectra and converted to vertical columns by division with an air mass factor (AMF) that accounts for the viewing geometry, atmospheric scattering, and the vertical profile of the gas (Palmer et al., 2001):

$$\mathrm{AMF} = \int_0^\infty w(z)s(z)\mathrm{d}z. \quad (2)$$

Here $w(z)$ is the scattering weight measuring the sensitivity of the retrieval to the gas concentration at altitude z, and $s(z)$ is a normalized vertical profile of gas number density. Here we recomputed the AMFs for the three retrievals using vertical profiles from GEOS-Chem, as it is necessary for comparing simulated and observed vertical columns (Duncan et al., 2014).

We remove observations impacted by the row anomaly (http://www.knmi.nl/omi/research/product/rowanomaly-background.php), and those with cloud fractions over 20 %. Previous validation of the OMI HCHO retrievals with SEAC^{4}RS aircraft observations revealed a

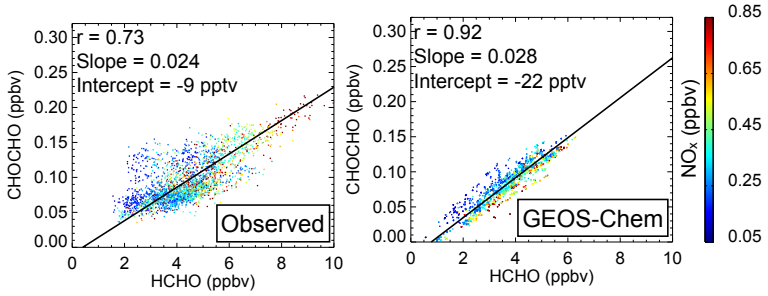

Figure 5. Relationship between CHOCHO and HCHO concentrations in the mixed layer (< 1 km a.g.l.) during SENEX (1 June–10 July 2013), color coded by NO_x concentration. Observed concentrations (Min et al., 2016; Cazorla et al., 2015) are compared to GEOS-Chem model values sampled along the flight tracks. Lines and reported slopes are from reduced major axis regressions.

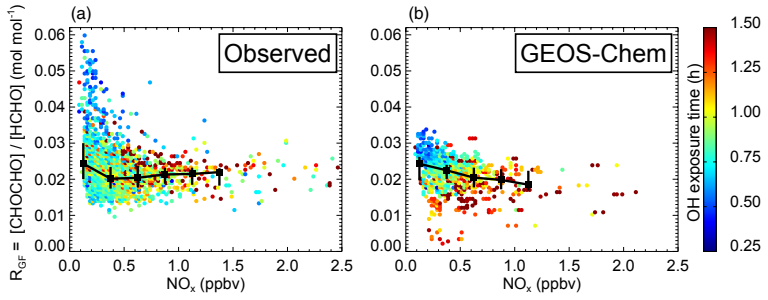

Figure 6. Dependence of the CHOCHO-to-HCHO ratio R_{GF} on NO_x concentrations for the SENEX conditions. Observations below 1 km altitude **(a)** are compared to GEOS-Chem model values sampled along the flight tracks **(b)**. Points are color coded by the OH exposure time t_{OH} (Eq. 1). Binned median and interquartile R_{GF} values in increments of 250 pptv NO_x for bins with more than 20 values are also shown.

43 % uniform low bias (Zhu et al., 2016), corrected in the data shown here.

Figure 7 compares CHOCHO and HCHO vertical columns from GEOS-Chem and OMI, and Fig. 8 shows spatial correlations over the eastern US. Excellent agreement is found for HCHO, providing an independent test of the correction to the OMI HCHO retrieval inferred from the SEAC^{4}RS data (Zhu et al., 2016). Since GEOS-Chem can also replicate the CHOCHO–HCHO correlation in the SENEX data, the simulated CHOCHO columns can be used to indirectly validate the OMI CHOCHO observations. CHOCHO from OMI is highly correlated with GEOS-Chem ($r = 0.81$), indicative of the isoprene source. However OMI CHOCHO shows a higher continental background and a factor of 2 weaker enhancement over the southeast US.

Zhu et al. (2016) suggested that errors in the assumed surface reflectivities affecting the AMFs were an important source of the bias in the OMI HCHO retrievals. CHOCHO retrievals are even more sensitive to surface reflectivity because of the longer wavelengths. Russell et al. (2011) previously pointed out that the OMI surface reflectivities used in the standard NO_2 retrievals (Kleipool et al., 2008) were too high and replaced them with high-resolution ($0.05° \times 0.05°$) reflectivity observations from MODIS (Schaaf and Wang, 2015) to produce the Berkeley High-Resolution (BEHR) OMI NO_2 retrieval. CHOCHO and NO_2 are retrieved at similar wavelengths so the sensitivity to surface reflectivity should be similar. Figure 7 (bottom right) shows the mean CHOCHO scattering weights computed from the OMI-SAO and BEHR. The lower BEHR surface reflectivity values result in a lower AMF and hence a higher vertical column (Fig. 7, bottom left panel). The slope of the regression between GEOS-Chem and OMI CHOCHO columns increases from 0.48 to 0.62, improving but not reconciling the differences.

As pointed out above, SENEX and other observations suggest that GEOS-Chem may be missing a background source of CHOCHO. Integration of the median CHOCHO profile above 2 km in Fig. 3 shows a negative model bias of 1.3×10^{14} molecules cm^{-2}, comparable to the continental background intercept in Fig. 8 (1.9×10^{14} molecules cm^{-2}). The nonzero intercept may in part reflect an underestimate of CHOCHO concentrations caused by a missing CHOCHO source over the southeast US, such as monoterpenes (Sect. 3). The presence of free-tropospheric CHOCHO would further impact the AMF calculation under continental background conditions since the retrieval sensitivity as measured by the scattering weights increases with altitude. Thus the retrieved continental background would be overestimated.

Figure 9 shows CHOCHO vs. HCHO relationships for OMI (using the BEHR scattering weights) and GEOS-Chem,

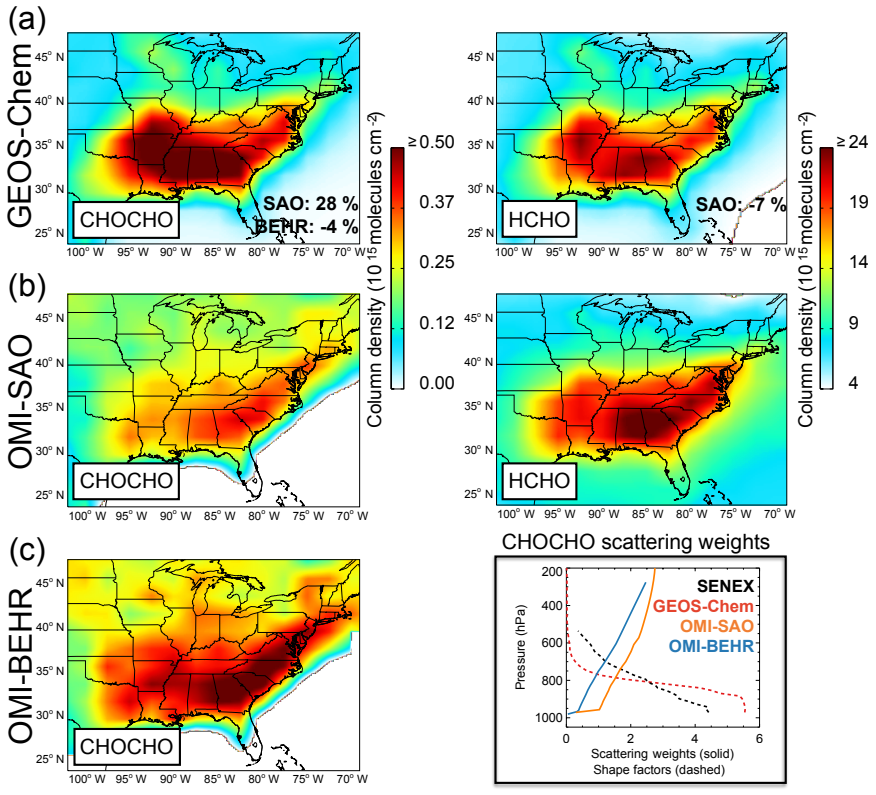

Figure 7. Mean CHOCHO and HCHO columns in summer (JJA) 2006–2007. GEOS-Chem model values **(a)** are compared to OMI satellite observations **(b, c)**. OMI-SAO is the standard operational product (Chan Miller et al., 2014; González Abad et al., 2015). The OMI-BEHR product for CHOCHO uses tropospheric scattering weights from the BEHR NO_2 retrieval (Russell et al., 2011; Laughner et al., 2016). The OMI HCHO observations have been scaled up by a factor of 1.67 to correct for retrieval bias (Zhu et al., 2016). The normalized mean bias (NMB) between GEOS-Chem and OMI in the southeast US (75–100° W, 29.5–37.5° N) is shown within the GEOS-Chem panels. The right panel of **(c)** shows the mean CHOCHO scattering weights (w) from the OMI-SAO and OMI-BEHR retrievals and the vertical shape factors (s) over the southeast US from the SENEX observations and GEOS-Chem in the southeast US from a typical orbit (10114, 9 June 2006).

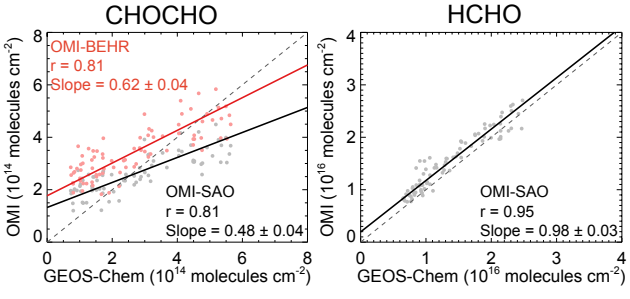

Figure 8. Scatterplots of OMI vs. GEOS-Chem CHOCHO and HCHO columns over the eastern US (75–100° W, 29.5–45° N). Values are seasonal means for JJA 2006–2007 as plotted in Fig. 7. OMI observations for CHOCHO are from the standard SAO retrieval (Chan Miller et al., 2014) and using BEHR scattering weights (Russell et al., 2011; Laughner et al., 2016). Correlation coefficients and reduced-major-axis (RMA) regressions are shown.

color coded by tropospheric NO_2 columns. Individual points are seasonal averages (data points from Fig. 7) in order to limit noise. The slope is steeper in GEOS-Chem because the CHOCHO columns are higher. Since GEOS-Chem reproduces the aircraft CHOCHO–HCHO relationship without bias (Fig. 5), this is further evidence of bias in the OMI CHOCHO observations. The CHOCHO–HCHO relationship is tight in both OMI ($r = 0.86$) and GEOS-Chem ($r = 0.99$), with no indication of a separate population of low-NO_x points with high R_{GF} as there was in the SENEX data. It thus appears from the OMI data that satellite observations of CHOCHO and HCHO in isoprene-dominated environments are redundant. This may reflect the higher NO_x levels in 2006–2007 compared to 2013 (Russell et al., 2012). However since median R_{GF} shows no significant variation with NO_x in the SENEX data (Fig. 6), the required temporal averaging of satellite observations is a more likely explanation for the tight correlation. Finer-scale and more temporally resolved data, as will be available from the TEMPO geostationary instrument to be launched in the 2018–2020 time

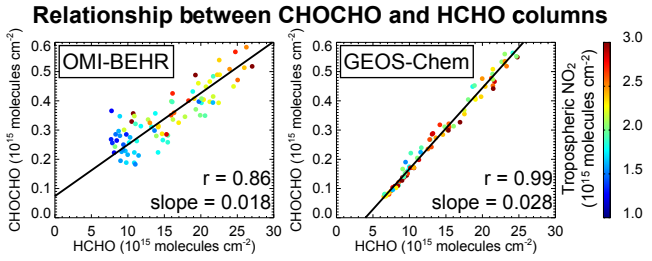

Figure 9. Relationship between CHOCHO and HCHO vertical columns over the eastern US (75–100° W, 29.5–45° N) in June–August 2006 and 2007 color coded by tropospheric NO_2 columns. OMI values with CHOCHO AMFs computed from BEHR scattering weights are compared to GEOS-Chem values. Lines and reported slopes are from reduced major axis regressions.

frame (Zoogman et al., 2016), may provide new perspectives of the utility of the CHOCHO retrieval.

5 Conclusions

We have used aircraft observations of glyoxal (CHOCHO), formaldehyde (HCHO), and related species from the SENEX aircraft campaign over the southeast US together with OMI satellite data to better understand the CHOCHO yield from isoprene and the complementarity of CHOCHO and HCHO observations from space for constraining isoprene emissions. This work includes a first validation of the CHOCHO retrieval from the OMI satellite instrument.

We began with an analysis of the time- and NO_x-dependent CHOCHO and HCHO yields from isoprene oxidation in the GEOS-Chem chemical transport model and in the Master Chemical Mechanism (MCMv3.3.1). The GEOS-Chem mechanism features several updates relevant to CHOCHO formation. These include a decrease in the δ-ISOPO$_2$ + NO branching ratio leading to prompt CHOCHO production under high-NO_x conditions, and a proposed low-NO_x pathway for prompt CHOCHO formation by photolysis of a dihydroperoxide dicarbonyl compound (DHDC) product from (1,5)H-shift isomerization of dihydroperoxy α-formyl peroxy radicals in the ISOPO$_2$ isomerization pathway (Fig. 1). GEOS-Chem and MCMv3.3.1 show similar HCHO yields from isoprene, increasing with increasing NO_x. CHOCHO yields from isoprene in MCMv3.3.1 show behavior similar to HCHO but GEOS-Chem has a higher yield at low NO_x from the ISOPO$_2$ isomerization pathway.

Comparison of GEOS-Chem to the SENEX observations of CHOCHO and HCHO shows good agreement in the boundary layer but a negative CHOCHO model bias in the free troposphere. This could reflect an instrument artifact but may also imply a missing background source in the model. Mixed layer (< 1 km) observations show a strong CHOCHO–HCHO relationship that is reproduced in GEOS-Chem and is remarkably consistent across all conditions except at very low NO_x where the [CHOCHO] / [HCHO] ratio (R_{GF}) can be unusually high. This reflects prompt formation of CHOCHO under low-NO_x conditions, which was missing from MCMv3.3.1 and is now simulated in our updated GEOS-Chem mechanism by DHDC photolysis. A previous model comparison to SENEX showed that MCMv3.3.1 underestimates the CHOCHO yield from isoprene (Li et al., 2016). Our work shows the missing DHDC production pathway can explain approximately 60 % of this underestimate, with the remainder caused by an underestimate of the δ-ISOPO$_2$ branching ratio (3.4 % in MCMv3.3.1 vs. 10 % in GEOS-Chem).

The SENEX observations enable indirect validation of the OMI CHOCHO satellite data using GEOS-Chem as an intercomparison platform. The OMI data show a continental background that is consistent with the SENEX free-tropospheric observations, and an enhancement over the southeast US that is consistent with the isoprene source. However this enhancement is a factor of 2 too low in the OMI data. A partial explanation is that surface reflectivities assumed in the standard OMI retrieval are too high. The satellite data show strong CHOCHO–HCHO correlation consistent with the model and imply that the two gases provide redundant information for constraining isoprene emissions in regions where isoprene is their dominant precursor. This redundancy may reflect the seasonal averaging in the OMI data required to reduce noise. Recent validation of the HCHO satellite data revealed negative retrieval biases (Zhu et al., 2016), which can be corrected using spatially uniform scaling factors (as done in this study). Since similar biases may exist for the CHOCHO retrieval, the scaled HCHO data should at present be preferentially used as proxy for isoprene emissions. Future geostationary observations from TEMPO (Zoogman et al., 2016) will require less temporal averaging and this may reveal the utility of CHOCHO observations for estimating isoprene emissions under low-NO_x conditions when isoprene oxidation is titrated.

Data availability. The SENEX observations used in this paper are publicly accessible online (https://esrl.noaa.gov/csd/groups/csd7/measurements/2013senex/). OMI CHOCHO, HCHO and NO_2 observations can be obtained from the Aura Validation Data Center (https://avdc.gsfc.nasa.gov/). Details on how to download GEOS-Chem source code can be found at http://www.geos-chem.org.

Competing interests. The authors declare that they have no conflict of interest.

The Supplement related to this article is available online at https://doi.org/10.5194/acp-17-8725-2017-supplement.

Acknowledgements. This work was funded by NASA ACMAP and ACCDAM and is a contribution to the NASA Aura Science Team. This research was undertaken with the assistance of resources provided at the NCI National Facility systems at the Australian National University through the National Computational Merit Allocation Scheme supported by the Australian Government. Jennifer Kaiser, Frank N. Keutsch, Glenn M. Wolfe, and Thomas F. Hanisco acknowledge support from the US EPA Science to Achieve Results (STAR) program (grant 83540601).

Edited by: Nga Lee Ng
Reviewed by: three anonymous referees

References

Abbot, D. S., Palmer, P. I., Martin, R. V., Chance, K. V., Jacob, D. J., and Guenther, A.: Seasonal and interannual variability of North American isoprene emissions as determined by formaldehyde column measurements from space, Geophys. Res. Lett., 30, 1886, https://doi.org/10.1029/2003GL017336, 2003.

Alvarado, L. M. A., Richter, A., Vrekoussis, M., Wittrock, F., Hilboll, A., Schreier, S. F., and Burrows, J. P.: An improved glyoxal retrieval from OMI measurements, Atmos. Meas. Tech., 7, 4133–4150, https://doi.org/10.5194/amt-7-4133-2014, 2014.

Baidar, S., Oetjen, H., Coburn, S., Dix, B., Ortega, I., Sinreich, R., and Volkamer, R.: The CU Airborne MAX-DOAS instrument: vertical profiling of aerosol extinction and trace gases, Atmos. Meas. Tech., 6, 719–739, https://doi.org/10.5194/amt-6-719-2013, 2013

Barkley, M. P., De Smedt, I., Van Roozendael, M., Kurosu, T. P., Chance, K., Arneth, A., Hagberg, D., Guenther, A., Paulot, F., Marais, E., and Mao, J.: Top-down isoprene emissions over tropical South America inferred from SCIAMACHY and OMI formaldehyde columns, J. Geophys. Res.-Atmos., 118, 6849–6868, https://doi.org/10.1002/jgrd.50552, 2013.

Bates, K. H., Crounse, J. D., Clair, J. M. S., Bennett, N. B., Nguyen, T. B., Seinfeld, J. H., Stoltz, B. M., and Wennberg, P. O.: Gas Phase Production and Loss of Isoprene Epoxydiols, J. Phys. Chem. A, 118, 1237–1246, https://doi.org/10.1021/jp4107958, 2014.

Browne, E. C. and Cohen, R. C.: Effects of biogenic nitrate chemistry on the NO_x lifetime in remote continental regions, Atmos. Chem. Phys., 12, 11917–11932, https://doi.org/10.5194/acp-12-11917-2012, 2012.

Bucsela, E. J., Krotkov, N. A., Celarier, E. A., Lamsal, L. N., Swartz, W. H., Bhartia, P. K., Boersma, K. F., Veefkind, J. P., Gleason, J. F., and Pickering, K. E.: A new stratospheric and tropospheric NO_2 retrieval algorithm for nadir-viewing satellite instruments: applications to OMI, Atmos. Meas. Tech., 6, 2607–2626, https://doi.org/10.5194/amt-6-2607-2013, 2013.

Carlton, A. G., Wiedinmyer, C., and Kroll, J. H.: A review of Secondary Organic Aerosol (SOA) formation from isoprene, Atmos. Chem. Phys., 9, 4987–5005, https://doi.org/10.5194/acp-9-4987-2009, 2009.

Cazorla, M., Wolfe, G. M., Bailey, S. A., Swanson, A. K., Arkinson, H. L., and Hanisco, T. F.: A new airborne laser-induced fluorescence instrument for in situ detection of formaldehyde throughout the troposphere and lower stratosphere, Atmos. Meas. Tech., 8, 541–552, https://doi.org/10.5194/amt-8-541-2015, 2015.

Chance, K., Palmer, P. I., Spurr, R. J. D., Martin, R. V., Kurosu, T. P., and Jacob, D. J.: Satellite observations of formaldehyde over North America from GOME, Geophys. Res. Lett., 27, 3461–3464, https://doi.org/10.1029/2000GL011857, 2000.

Chan Miller, C., Gonzalez Abad, G., Wang, H., Liu, X., Kurosu, T., Jacob, D. J., and Chance, K.: Glyoxal retrieval from the Ozone Monitoring Instrument, Atmos. Meas. Tech., 7, 3891–3907, https://doi.org/10.5194/amt-7-3891-2014, 2014.

Chan Miller, C., Jacob, D. J., González Abad, G., and Chance, K.: Hotspot of glyoxal over the Pearl River delta seen from the OMI satellite instrument: implications for emissions of aromatic hydrocarbons, Atmos. Chem. Phys., 16, 4631–4639, https://doi.org/10.5194/acp-16-4631-2016, 2016.

Crounse, J. D., Paulot, F., Kjaergaard, H. G., and Wennberg, P. O.: Peroxy radical isomerization in the oxidation of isoprene, Phys. Chem. Chem. Phys., 13, 13607–13613, https://doi.org/10.1039/C1CP21330J, 2011.

Crounse, J. D., Nielsen, L. B., Jørgensen, S., Kjaergaard, H. G., and Wennberg, P. O.: Autoxidation of Organic Compounds in the Atmosphere, The J. Phys. Chem. Lett., 4, 3513–3520, https://doi.org/10.1021/jz4019207, 2013.

Curci, G., Palmer, P. I., Kurosu, T. P., Chance, K., and Visconti, G.: Estimating European volatile organic compound emissions using satellite observations of formaldehyde from the Ozone Monitoring Instrument, Atmos. Chem. Phys., 10, 11501–11517, https://doi.org/10.5194/acp-10-11501-2010, 2010.

de Gouw, J. and Warneke, C.: Measurements of volatile organic compounds in the earth's atmosphere using proton-transfer-reaction mass spectrometry, Mass Spectrom. Rev., 26, 223–257, https://doi.org/10.1002/mas.20119, 2007.

DiGangi, J. P., Henry, S. B., Kammrath, A., Boyle, E. S., Kaser, L., Schnitzhofer, R., Graus, M., Turnipseed, A., Park, J.-H., Weber, R. J., Hornbrook, R. S., Cantrell, C. A., Maudlin III, R. L., Kim, S., Nakashima, Y., Wolfe, G. M., Kajii, Y., Apel, E. C., Goldstein, A. H., Guenther, A., Karl, T., Hansel, A., and Keutsch, F. N.: Observations of glyoxal and formaldehyde as metrics for the anthropogenic impact on rural photochemistry, Atmos. Chem. Phys., 12, 9529–9543, https://doi.org/10.5194/acp-12-9529-2012, 2012.

Duncan, B. N., Prados, A. I., Lamsal, L. N., Liu, Y., Streets, D. G., Gupta, P., Hilsenrath, E., Kahn, R. A., Nielsen, J. E., Beyersdorf, A. J., Burton, S. P., Fiore, A. M., Fishman, J., Henze, D. K., Hostetler, C. A., Krotkov, N. A., Lee, P., Lin, M., Pawson, S., Pfister, G., Pickering, K. E., Pierce, R. B., Yoshida, Y., and Ziemba, L. D.: Satellite data of atmospheric pollution for U.S. air quality applications: Examples of applications, summary of data end-user resources, answers to FAQs, and common mistakes to avoid, Atmos. Environ., 94, 647–662, https://doi.org/10.1016/j.atmosenv.2014.05.061, 2014.

Emmerson, K. M. and Evans, M. J.: Comparison of tropospheric gas-phase chemistry schemes for use within global models, Atmos. Chem. Phys., 9, 1831–1845, https://doi.org/10.5194/acp-9-1831-2009, 2009.

Fisher, J. A., Jacob, D. J., Travis, K. R., Kim, P. S., Marais, E. A., Chan Miller, C., Yu, K., Zhu, L., Yantosca, R. M., Sulprizio, M. P., Mao, J., Wennberg, P. O., Crounse, J. D., Teng, A. P., Nguyen, T. B., St. Clair, J. M., Cohen, R. C., Romer,

P., Nault, B. A., Wooldridge, P. J., Jimenez, J. L., Campuzano-Jost, P., Day, D. A., Hu, W., Shepson, P. B., Xiong, F., Blake, D. R., Goldstein, A. H., Misztal, P. K., Hanisco, T. F., Wolfe, G. M., Ryerson, T. B., Wisthaler, A., and Mikoviny, T.: Organic nitrate chemistry and its implications for nitrogen budgets in an isoprene- and monoterpene-rich atmosphere: constraints from aircraft (SEAC^{4}RS) and ground-based (SOAS) observations in the Southeast US, Atmos. Chem. Phys., 16, 5969–5991, https://doi.org/10.5194/acp-16-5969-2016, 2016.

Fortems-Cheiney, A., Chevallier, F., Pison, I., Bousquet, P., Saunois, M., Szopa, S., Cressot, C., Kurosu, T. P., Chance, K., and Fried, A.: The formaldehyde budget as seen by a global-scale multi-constraint and multi-species inversion system, Atmos. Chem. Phys., 12, 6699–6721, https://doi.org/10.5194/acp-12-6699-2012, 2012.

Fu, T.-M., Jacob, D. J., Palmer, P. I., Chance, K., Wang, Y. X., Barletta, B., Blake, D. R., Stanton, J. C., and Pilling, M. J.: Space-based formaldehyde measurements as constraints on volatile organic compound emissions in east and south Asia and implications for ozone, J. Geophys. Res., 112, D06312, https://doi.org/10.1029/2006JD007853, 2007.

Fu, T.-M., Jacob, D. J., Wittrock, F., Burrows, J. P., Vrekoussis, M., and Henze, D. K.: Global budgets of atmospheric glyoxal and methylglyoxal, and implications for formation of secondary organic aerosols, J. Geophys. Res., 113, D15303, https://doi.org/10.1029/2007JD009505, 2008.

Galloway, M. M., Huisman, A. J., Yee, L. D., Chan, A. W. H., Loza, C. L., Seinfeld, J. H., and Keutsch, F. N.: Yields of oxidized volatile organic compounds during the OH radical initiated oxidation of isoprene, methyl vinyl ketone, and methacrolein under high-NO_x conditions, Atmos. Chem. Phys., 11, 10779-10790, https://doi.org/10.5194/acp-11-10779-2011, 2011.

Geng, F., Tie, X., Guenther, A., Li, G., Cao, J., and Harley, P.: Effect of isoprene emissions from major forests on ozone formation in the city of Shanghai, China, Atmos. Chem. Phys., 11, 10449–10459, https://doi.org/10.5194/acp-11-10449-2011, 2011.

González Abad, G., Liu, X., Chance, K., Wang, H., Kurosu, T. P., and Suleiman, R.: Updated Smithsonian Astrophysical Observatory Ozone Monitoring Instrument (SAO OMI) formaldehyde retrieval, Atmos. Meas. Tech., 8, 19–32, https://doi.org/10.5194/amt-8-19-2015, 2015.

Guenther, A. B., Jiang, X., Heald, C. L., Sakulyanontvittaya, T., Duhl, T., Emmons, L. K., and Wang, X.: The Model of Emissions of Gases and Aerosols from Nature version 2.1 (MEGAN2.1): an extended and updated framework for modeling biogenic emissions, Geosci. Model Dev., 5, 1471–1492, https://doi.org/10.5194/gmd-5-1471-2012, 2012.

Jenkin, M. E., Young, J. C., and Rickard, A. R.: The MCM v3.3.1 degradation scheme for isoprene, Atmos. Chem. Phys., 15, 11433–11459, https://doi.org/10.5194/acp-15-11433-2015, 2015.

Kaiser, J., Wolfe, G. M., Min, K. E., Brown, S. S., Miller, C. C., Jacob, D. J., deGouw, J. A., Graus, M., Hanisco, T. F., Holloway, J., Peischl, J., Pollack, I. B., Ryerson, T. B., Warneke, C., Washenfelder, R. A., and Keutsch, F. N.: Reassessing the ratio of glyoxal to formaldehyde as an indicator of hydrocarbon precursor speciation, Atmos. Chem. Phys., 15, 7571–7583, https://doi.org/10.5194/acp-15-7571-2015, 2015.

Kim, P. S., Jacob, D. J., Fisher, J. A., Travis, K., Yu, K., Zhu, L., Yantosca, R. M., Sulprizio, M. P., Jimenez, J. L., Campuzano-Jost, P., Froyd, K. D., Liao, J., Hair, J. W., Fenn, M. A., Butler, C. F., Wagner, N. L., Gordon, T. D., Welti, A., Wennberg, P. O., Crounse, J. D., St. Clair, J. M., Teng, A. P., Millet, D. B., Schwarz, J. P., Markovic, M. Z., and Perring, A. E.: Sources, seasonality, and trends of southeast US aerosol: an integrated analysis of surface, aircraft, and satellite observations with the GEOS-Chem chemical transport model, Atmos. Chem. Phys., 15, 10411–10433, https://doi.org/10.5194/acp-15-10411-2015, 2015.

Kleipool, Q. L., Dobber, M. R., de Haan, J. F., and Levelt, P. F.: Earth surface reflectance climatology from 3 years of OMI data, J. Geophys. Res.-Atmos., 113, D18308, https://doi.org/10.1029/2008JD010290, 008.

Laughner, J. L., Zare, A., and Cohen, R. C.: Effects of daily meteorology on the interpretation of space-based remote sensing of NO_2, Atmos. Chem. Phys., 16, 15247–15264, https://doi.org/10.5194/acp-16-15247-2016, 2016.

Lee, Y.-N., Zhou, X., Kleinman, L. I., Nunnermacker, L. J., Springston, S. R., Daum, P. H., Newman, L., Keigley, W. G., Holdren, M. W., Spicer, C. W., Young, V., Fu, B., Parrish, D. D., Holloway, J., Williams, J., Roberts, J. M., Ryerson, T. B., and Fehsenfeld, F. C.: Atmospheric chemistry and distribution of formaldehyde and several multioxygenated carbonyl compounds during the 1995 Nashville/Middle Tennessee Ozone Study, J. Geophys. Res.-Atmos., 103, 22449–22462, https://doi.org/10.1029/98JD01251, 1998.

Li, J., Mao, J., Min, K.-E., Washenfelder, R. A., Brown, S. S., Kaiser, J., Keutsch, F. N., Volkamer, R., Wolfe, G. M., Hanisco, T. F., Pollack, I. B., Ryerson, T. B., Graus, M., Gilman, J. B., Lerner, B. M., Warneke, C., de Gouw, J. A., Middlebrook, A. M., Liao, J., Welti, A., Henderson, B. H., McNeill, V. F., Hall, S. R., Ullmann, K., Donner, L. J., Paulot, F., and Horowitz, L. W.: Observational constraints on glyoxal production from isoprene oxidation and its contribution to organic aerosol over the Southeast United States, J. Geophys. Res.-Atmos., 121, 9849–9861, https://doi.org/10.1002/2016JD025331, 2016.

Madronich, S.: Photodissociation in the atmosphere: 1. Actinic flux and the effects of ground reflections and clouds, J. Geophys. Res.-Atmos., 92, 9740–9752, https://doi.org/10.1029/JD092iD08p09740, 1987.

Mao, J., Paulot, F., Jacob, D. J., Cohen, R. C., Crounse, J. D., Wennberg, P. O., Keller, C. A., Hudman, R. C., Barkley, M. P., and Horowitz, L. W.: Ozone and organic nitrates over the eastern United States: Sensitivity to isoprene chemistry, J. Geophys. Res.-Atmos., 118, 11256–11268, https://doi.org/10.1002/jgrd.50817, 2013.

Marais, E. A., Jacob, D. J., Kurosu, T. P., Chance, K., Murphy, J. G., Reeves, C., Mills, G., Casadio, S., Millet, D. B., Barkley, M. P., Paulot, F., and Mao, J.: Isoprene emissions in Africa inferred from OMI observations of formaldehyde columns, Atmos. Chem. Phys., 12, 6219–6235, https://doi.org/10.5194/acp-12-6219-2012, 2012.

Marais, E. A., Jacob, D. J., Jimenez, J. L., Campuzano-Jost, P., Day, D. A., Hu, W., Krechmer, J., Zhu, L., Kim, P. S., Miller, C. C., Fisher, J. A., Travis, K., Yu, K., Hanisco, T. F., Wolfe, G. M., Arkinson, H. L., Pye, H. O. T., Froyd, K. D., Liao, J., and McNeill, V. F.: Aqueous-phase mechanism for secondary or-

ganic aerosol formation from isoprene: application to the southeast United States and co-benefit of SO_2 emission controls, Atmos. Chem. Phys., 16, 1603–1618, https://doi.org/10.5194/acp-16-1603-2016, 2016.

Millet, D. B., Jacob, D. J., Boersma, K. F., Fu, T.-M., Kurosu, T. P., Chance, K., Heald, C. L., and Guenther, A.: Spatial distribution of isoprene emissions from North America derived from formaldehyde column measurements by the OMI satellite sensor, J. Geophys. Res.-Atmos., 113, D02307, https://doi.org/10.1029/2007JD008950, 2008.

Min, K.-E., Washenfelder, R. A., Dubé, W. P., Langford, A. O., Edwards, P. M., Zarzana, K. J., Stutz, J., Lu, K., Rohrer, F., Zhang, Y., and Brown, S. S.: A broadband cavity enhanced absorption spectrometer for aircraft measurements of glyoxal, methylglyoxal, nitrous acid, nitrogen dioxide, and water vapor, Atmos. Meas. Tech., 9, 423–440, https://doi.org/10.5194/amt-9-423-2016, 2016.

Molod, A., Takacs, L., Suarez, M., Bacmeister, J., Song, I.-S., and Eichmann, A.: The GEOS-5 Atmospheric General Circulation Model: Mean Climate and Development from MERRA to Fortuna, Tech. Rep. NASA/TM–2012-104606/Vol 28, Nasa Godard Space Flight Center, 2012.

Müller, J.-F., Peeters, J., and Stavrakou, T.: Fast photolysis of carbonyl nitrates from isoprene, Atmos. Chem. Phys., 14, 2497–2508, https://doi.org/10.5194/acp-14-2497-2014, 2014.

Palmer, P. I., Jacob, D. J., Chance, K., Martin, R. V., Spurr, R. J. D., Kurosu, T. P., Bey, I., Yantosca, R., Fiore, A., and Li, Q.: Air mass factor formulation for spectroscopic measurements from satellites: Application to formaldehyde retrievals from the Global Ozone Monitoring Experiment, J. Geophys. Res.-Atmos., 106, 14539–14550, https://doi.org/10.1029/2000JD900772, 2001.

Palmer, P. I., Jacob, D. J., Fiore, A. M., Martin, R. V., Chance, K., and Kurosu, T. P.: Mapping isoprene emissions over North America using formaldehyde column observations from space, J. Geophys. Res.-Atmos., 108, 4180, https://doi.org/10.1029/2002JD002153, 2003.

Palmer, P. I., Abbot, D. S., Fu, T.-M., Jacob, D. J., Chance, K., Kurosu, T. P., Guenther, A., Wiedinmyer, C., Stanton, J. C., Pilling, M. J., Pressley, S. N., Lamb, B., and Sumner, A. L.: Quantifying the seasonal and interannual variability of North American isoprene emissions using satellite observations of the formaldehyde column, J. Geophys. Res.-Atmos., 111, D12315, https://doi.org/10.1029/2005JD006689, 2006.

Paulot, F., Crounse, J. D., Kjaergaard, H. G., Kroll, J. H., Seinfeld, J. H., and Wennberg, P. O.: Isoprene photooxidation: new insights into the production of acids and organic nitrates, Atmos. Chem. Phys., 9, 1479–1501, https://doi.org/10.5194/acp-9-1479-2009, 2009a.

Paulot, F., Crounse, J. D., Kjaergaard, H. G., Kürten, A., St. Clair, J. M., Seinfeld, J. H., and Wennberg, P. O.: Unexpected Epoxide Formation in the Gas-Phase Photooxidation of Isoprene, Science, 325, 730–733, https://doi.org/10.1126/science.1172910, 2009b.

Peeters, J. and Muller, J.-F.: HO_x radical regeneration in isoprene oxidation via peroxy radical isomerisations. II: experimental evidence and global impact, Phys. Chem. Chem. Phys., 12, 14227–14235, https://doi.org/10.1039/C0CP00811G, 2010.

Peeters, J., Nguyen, T. L., and Vereecken, L.: HO_x radical regeneration in the oxidation of isoprene, Phys. Chem. Chem. Phys., 11, 5935–5939, https://doi.org/10.1039/B908511D, 2009.

Peeters, J., Müller, J.-F., Stavrakou, T., and Nguyen, V. S.: Hydroxyl Radical Recycling in Isoprene Oxidation Driven by Hydrogen Bonding and Hydrogen Tunneling: The Upgraded LIM1 Mechanism, J. Phys. Chem. A, 118, 8625–8643, https://doi.org/10.1021/jp5033146, 2014.

Pollack, I. B., Lerner, B. M., and Ryerson, T. B.: Evaluation of ultraviolet light-emitting diodes for detection of atmospheric NO_2 by photolysis – chemiluminescence, J. Atmos. Chem., 65, 111–125, https://doi.org/10.1007/s10874-011-9184-3, 2010.

Russell, A. R., Perring, A. E., Valin, L. C., Bucsela, E. J., Browne, E. C., Wooldridge, P. J., and Cohen, R. C.: A high spatial resolution retrieval of NO_2 column densities from OMI: method and evaluation, Atmos. Chem. Phys., 11, 8543–8554, https://doi.org/10.5194/acp-11-8543-2011, 2011.

Russell, A. R., Valin, L. C., and Cohen, R. C.: Trends in OMI NO_2 observations over the United States: effects of emission control technology and the economic recession, Atmos. Chem. Phys., 12, 12197–12209, https://doi.org/10.5194/acp-12-12197-2012, 2012.

Ryerson, T. B., Huey, L. G., Knapp, K., Neuman, J. A., Parrish, D. D., Sueper, D. T., and Fehsenfeld, F. C.: Design and initial characterization of an inlet for gas-phase NO_y measurements from aircraft, J. Geophys. Res.-Atmos., 104, 5483–5492, https://doi.org/10.1029/1998JD100087, 1999.

Schaaf, C. and Wang, Z.: MCD43C3 MODIS/Terra+Aqua BRDF/Albedo Albedo Daily L3 Global 0.05Deg CMG V006., Tech. Rep., https://doi.org/10.5067/MODIS/MCD43C3.006, NASA EOSDIS Land Processes DAAC, 2015.

Stavrakou, T., Peeters, J., and Müller, J.-F.: Improved global modelling of HO_x recycling in isoprene oxidation: evaluation against the GABRIEL and INTEX-A aircraft campaign measurements, Atmos. Chem. Phys., 10, 9863–9878, https://doi.org/10.5194/acp-10-9863-2010, 2010.

Travis, K. R., Jacob, D. J., Fisher, J. A., Kim, P. S., Marais, E. A., Zhu, L., Yu, K., Miller, C. C., Yantosca, R. M., Sulprizio, M. P., Thompson, A. M., Wennberg, P. O., Crounse, J. D., St. Clair, J. M., Cohen, R. C., Laughner, J. L., Dibb, J. E., Hall, S. R., Ullmann, K., Wolfe, G. M., Pollack, I. B., Peischl, J., Neuman, J. A., and Zhou, X.: Why do models overestimate surface ozone in the Southeast United States?, Atmos. Chem. Phys., 16, 13561–13577, https://doi.org/10.5194/acp-16-13561-2016, 2016.

Volkamer, R., Platt, U., and Wirtz, K.: Primary and Secondary Glyoxal Formation from Aromatics: Experimental Evidence for the Bicycloalkyl-Radical Pathway from Benzene, Toluene, and p-Xylene, J. Phys. Chem. A, 105, 7865–7874, https://doi.org/10.1021/jp010152w, 2001.

Volkamer, R., Baidar, S., Campos, T. L., Coburn, S., DiGangi, J. P., Dix, B., Eloranta, E. W., Koenig, T. K., Morley, B., Ortega, I., Pierce, B. R., Reeves, M., Sinreich, R., Wang, S., Zondlo, M. A., and Romashkin, P. A.: Aircraft measurements of BrO, IO, glyoxal, NO_2, H_2O, O_2-O_2 and aerosol extinction profiles in the tropics: comparison with aircraft-/ship-based in situ and lidar measurements, Atmos. Meas. Tech., 8, 2121–2148, https://doi.org/10.5194/amt-8-2121-2015, 2015.

Vrekoussis, M., Wittrock, F., Richter, A., and Burrows, J. P.: Temporal and spatial variability of glyoxal as observed from space, Atmos. Chem. Phys., 9, 4485–4504, https://doi.org/10.5194/acp-9-4485-2009, 2009.

Vrekoussis, M., Wittrock, F., Richter, A., and Burrows, J. P.: GOME-2 observations of oxygenated VOCs: what can we learn from the ratio glyoxal to formaldehyde on a global scale?, Atmos. Chem. Phys., 10, 10145–10160, https://doi.org/10.5194/acp-10-10145-2010, 2010.

Wagner, N. L., Brock, C. A., Angevine, W. M., Beyersdorf, A., Campuzano-Jost, P., Day, D., de Gouw, J. A., Diskin, G. S., Gordon, T. D., Graus, M. G., Holloway, J. S., Huey, G., Jimenez, J. L., Lack, D. A., Liao, J., Liu, X., Markovic, M. Z., Middlebrook, A. M., Mikoviny, T., Peischl, J., Perring, A. E., Richardson, M. S., Ryerson, T. B., Schwarz, J. P., Warneke, C., Welti, A., Wisthaler, A., Ziemba, L. D., and Murphy, D. M.: In situ vertical profiles of aerosol extinction, mass, and composition over the southeast United States during SENEX and SEAC^{4}RS: observations of a modest aerosol enhancement aloft, Atmos. Chem. Phys., 15, 7085–7102, https://doi.org/10.5194/acp-15-7085-2015, 2015.

Warneke, C., Trainer, M., de Gouw, J. A., Parrish, D. D., Fahey, D. W., Ravishankara, A. R., Middlebrook, A. M., Brock, C. A., Roberts, J. M., Brown, S. S., Neuman, J. A., Lerner, B. M., Lack, D., Law, D., Hübler, G., Pollack, I., Sjostedt, S., Ryerson, T. B., Gilman, J. B., Liao, J., Holloway, J., Peischl, J., Nowak, J. B., Aikin, K. C., Min, K.-E., Washenfelder, R. A., Graus, M. G., Richardson, M., Markovic, M. Z., Wagner, N. L., Welti, A., Veres, P. R., Edwards, P., Schwarz, J. P., Gordon, T., Dube, W. P., McKeen, S. A., Brioude, J., Ahmadov, R., Bougiatioti, A., Lin, J. J., Nenes, A., Wolfe, G. M., Hanisco, T. F., Lee, B. H., Lopez-Hilfiker, F. D., Thornton, J. A., Keutsch, F. N., Kaiser, J., Mao, J., and Hatch, C. D.: Instrumentation and measurement strategy for the NOAA SENEX aircraft campaign as part of the Southeast Atmosphere Study 2013, Atmos. Meas. Tech., 9, 3063–3093, https://doi.org/10.5194/amt-9-3063-2016, 2016.

Wittrock, F., Richter, A., Oetjen, H., Burrows, J. P., Kanakidou, M., Myriokefalitakis, S., Volkamer, R., Beirle, S., Platt, U., and Wagner, T.: Simultaneous global observations of glyoxal and formaldehyde from space, Geophys. Res. Lett., 33, L16804, https://doi.org/10.1029/2006GL026310, 2006.

Wolfe, G. M., Kaiser, J., Hanisco, T. F., Keutsch, F. N., de Gouw, J. A., Gilman, J. B., Graus, M., Hatch, C. D., Holloway, J., Horowitz, L. W., Lee, B. H., Lerner, B. M., Lopez-Hilifiker, F., Mao, J., Marvin, M. R., Peischl, J., Pollack, I. B., Roberts, J. M., Ryerson, T. B., Thornton, J. A., Veres, P. R., and Warneke, C.: Formaldehyde production from isoprene oxidation across NO_x regimes, Atmos. Chem. Phys., 16, 2597–2610, https://doi.org/10.5194/acp-16-2597-2016, 2016.

Yu, K., Jacob, D. J., Fisher, J. A., Kim, P. S., Marais, E. A., Miller, C. C., Travis, K. R., Zhu, L., Yantosca, R. M., Sulprizio, M. P., Cohen, R. C., Dibb, J. E., Fried, A., Mikoviny, T., Ryerson, T. B., Wennberg, P. O., and Wisthaler, A.: Sensitivity to grid resolution in the ability of a chemical transport model to simulate observed oxidant chemistry under high-isoprene conditions, Atmos. Chem. Phys., 16, 4369–4378, https://doi.org/10.5194/acp-16-4369-2016, 2016.

Zhu, L., Jacob, D. J., Kim, P. S., Fisher, J. A., Yu, K., Travis, K. R., Mickley, L. J., Yantosca, R. M., Sulprizio, M. P., De Smedt, I., González Abad, G., Chance, K., Li, C., Ferrare, R., Fried, A., Hair, J. W., Hanisco, T. F., Richter, D., Jo Scarino, A., Walega, J., Weibring, P., and Wolfe, G. M.: Observing atmospheric formaldehyde (HCHO) from space: validation and intercomparison of six retrievals from four satellites (OMI, GOME2A, GOME2B, OMPS) with SEAC^{4}RS aircraft observations over the southeast US, Atmos. Chem. Phys., 16, 13477–13490, https://doi.org/10.5194/acp-16-13477-2016, 2016.

Zoogman, P., Liu, X., Suleiman, R., Pennington, W., Flittner, D., Al-Saadi, J., Hilton, B., Nicks, D., Newchurch, M., Carr, J., Janz, S., Andraschko, M., Arola, A., Baker, B., Canova, B., Miller, C. C., Cohen, R., Davis, J., Dussault, M., Edwards, D., Fishman, J., Ghulam, A., Abad, G. G., Grutter, M., Herman, J., Houck, J., Jacob, D., Joiner, J., Kerridge, B., Kim, J., Krotkov, N., Lamsal, L., Li, C., Lindfors, A., Martin, R., McElroy, C., McLinden, C., Natraj, V., Neil, D., Nowlan, C., O'Sullivan, E., Palmer, P., Pierce, R., Pippin, M., Saiz-Lopez, A., Spurr, R., Szykman, J., Torres, O., Veefkind, J., Veihelmann, B., Wang, H., Wang, J., and Chance, K.: Tropospheric emissions: Monitoring of pollution (TEMPO), J. Quant. Spectrosc. Ra., 186, 17–39, https://doi.org/10.1016/j.jqsrt.2016.05.008, 2016.

Supplement of Atmos. Chem. Phys., 17, 8725–8738, 2017
https://doi.org/10.5194/acp-17-8725-2017-supplement

Atmospheric Chemistry and Physics
Open Access
EGU

Supplement of

Glyoxal yield from isoprene oxidation and relation to formaldehyde: chemical mechanism, constraints from SENEX aircraft observations, and interpretation of OMI satellite data

Christopher Chan Miller et al.

Correspondence to: Daniel J. Jacob (djacob@fas.harvard.edu)

Table S1: Summary of the suggested changes to the GEOS-Chem chemical mechanism inferred from our analysis of SENEX observations.

Reaction	Base Model Products	Revised Model Products	Base & Revised Reaction Rates
RIO2→	HPALD	0.5HPALD + 0.5DHPCARP	$k = 4.07 \times 10^{8} \exp\left(\frac{-7694}{T}\right)$
DHPCARP+NO→	no reaction	GLYX + MGLY + NO2 + OH	$k = 2.7 \times 10^{-12} \exp\left(\frac{360}{T}\right)$
DHPCARP+HO2→	no reaction	RCOOH	$k = 2.05 \times 10^{-13} \exp\left(\frac{1300}{T}\right)$
DHPCARP→	no reaction	RCOOH + CO + OH	$k = 2.9 \times 10^{7} \exp\left(\frac{-5300}{T}\right)$
DHPCARP→	no reaction	DHDC	$k = 1.28 \times 10^{7} \exp\left(\frac{-5300}{T}\right)$
DHDC+$h\nu$ →	no reaction	MGLY + GLYX + 2OH	J_{HPALD}
HPALD+OH→	MGLY + CO + CH2O + OH	0.365HPC52O2 + 0.085GLYX + 0.085MCO3 + 0.55MGLY + 0.55CO + 0.55CH2O + 0.635OH	$k = 5.11 \times 10^{-11}$
HPALD+$h\nu$ →	0.25GLYX + 0.25MGLY + 0.5HAC + 0.5GLYC + CH2O + HO2 + OH	0.5MGLY + 0.39HAC + 0.11GLYC + 0.11MCO3 + 1.89CO + 0.89HO2 + 2OH	J_{HPALD}
HPC52O2+NO→	no reaction	GLYX + MGLY + NO2 + HO2	$k = 2.7 \times 10^{-12} \exp\left(\frac{360}{T}\right)$
HPC52O2+HO2→	no reaction	RCOOH	$k = 2.05 \times 10^{-13} \exp\left(\frac{1300}{T}\right)$
RIO2+NO→	0.93NO2 + 0.855HO2 + 0.71CH2O + 0.414MVK + 0.296MACR + 0.023ISOPND + 0.047ISOPNB + 0.145HC5 + 0.075DIBOO	0.91NO2 + 0.82HO2 + 0.82CH2O + 0.476MVK + 0.344MACR + 0.009ISOPND + 0.081ISOPNB + 0.058HC5 + 0.03DIBOO †	$k = 2.7 \times 10^{-12} \exp\left(\frac{350}{T}\right)$
GLYC+OH→	f(0.732CH2O + 0.5CO + 0.227OH + 0.773HO2 + 0.134GLYX + 0.134HCOOH) + (1-f)(HCOOH + OH + CO)	0.676CH2O + 0.466CO + 0.21OH + 0.79HO2 + 0.2GLYX + 0.124HCOOH	$k = 8 \times 10^{-12}$ $f = 1 - 11.0729 \exp\left(\frac{-T}{73}\right)$

†The revised mechanism has been updated to include the isoprene nitrate yield recommendation by Fisher et al. [2016]. The reaction used in this study preserved the ISOPNB and ISOPND yields from the GEOS-Chem mechanism (RIO2+NO→0.936NO2 + 0.904HO2 + 0.844CH2O + 0.493MVK + 0.351MACR + 0.01ISOPND + 0.056ISOPNB + 0.06HC5 + 0.03DIBOO). The difference CHOCHO production from isoprene over the southeast US due to this change is less than 2%, howeer it is important for isoprene organic nitrates.

S1 Production of CHOCHO from glycolaldehyde

The main two sinks of glycolaldehyde in the atmosphere are via photolysis and OH, with the latter oxidation pathway yielding CHOCHO. Reported yields of CHOCHO via OH initiated GLYC oxidation range from 14 - 29% [Magneron et al., 2005, Butkovskaya et al., 2006, Chan et al., 2009, Galloway et al., 2011]. Here we use a yield of 20%, following MCMv3.3.1, whose yield value is from Magneron et al. [2005]. Li et al. [2016] set the yield in AM3 to 13% citing Butkovskaya et al. [2006], and report an absolute yield from GLYC oxidation of 7.2%. If this yield is constant, this implies that 45% of GLYC in AM3 is lost to photolysis. However photolysis is generally a minor GLYC sink. Figure S1 shows the fraction of GLYC lost to OH simulated by GEOS-Chem over the SENEX period (June 1-July 10 2013). This simulation is from the model as described in the main text, except that it was performed globally at $2^\circ \times 2.5^\circ$ degree resolution. The model suggests approximately 20% of GLYC is lost to photolysis over the Southeast US, a factor of 2.5 smaller than suggested by the absolute yield from Li et al. [2016].

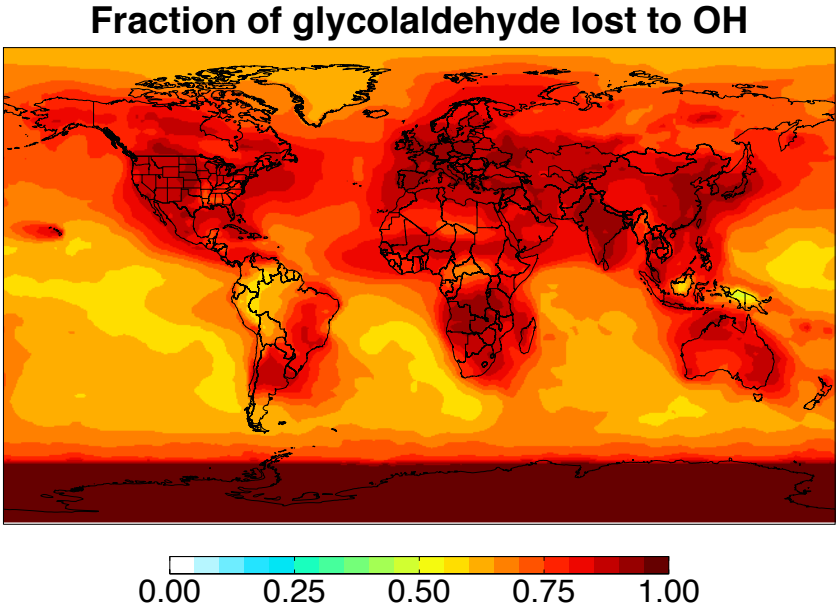

Figure S1: The fraction of GLYC lost to oxidation by OH for the period 1 June - 10 July 2013, simulated by GEOS-Chem.

Butkovskaya et al. [2006] observed that the yield of CHOCHO from OH initiated GLYC oxidation decreased with decreasing temperature. Both our GEOS-Chem mechanism and the AM3 mechanism derive from the mechanism presented by Mao et al. [2013]. Here, the CHOCHO yield from GLYC + OH was calculated from a temperature dependent parameterization of the yields from Butkovskaya et al. [2006] (Table S1). Figure S2 shows the CHOCHO yield from OH initiated GLYC oxidation as a function of temperature in the original and revised GEOS-Chem mechanisms. The parameterization tends to underestimate the CHOCHO yield compared to the chamber study it was based on (e.g. 296K Butkovskaya

et al. [2006] report a 14% yield, compared to 10.8% in the parameterization). The yield from the parameterization is approximately half that from the MCMv3.3.1 reaction implemented in this study, and thus could explain the difference in GLYC yields shown here and for AM3, if this is the actual reaction implemented.

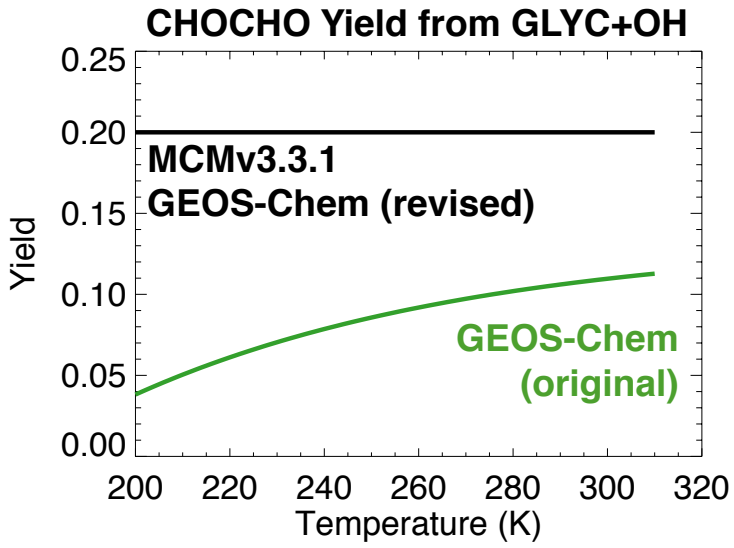

Figure S2: CHOCHO yield from the reaction of GLYC with OH as a function of temperature, from the original and revised GEOS-Chem mechanism presented in Table S1

S2 Production of CHOCHO from Isoprene epoxydiols

$\beta-$isoprene epoxydiols (IEPOXB, Figure S3) account for $\sim$ 95% of total IEPOX [Jenkin et al., 2015]. The IEPOXB pathways pertinent to CHOCHO production from MCMv3.3.1 are shown in Figure S3. The H-abstraction pathway leading to CHOCHO production via C58AO2 accounts for 37% of IEPOXB loss to OH, and is based on IEPOX chamber experiements [Bates et al., 2014]. CHOCHO forms as a coproduct to hydroxyacetone (ACETOL) via reaction with NO. In MCMv3.3.1 the reaction between C58AO2 and HO_2 leads to the generation of the assocated hydroperoxide (C58AOOH). Li et al. [2016] suggest that MCMv3.3.1 underestimates the CHOCHO yield from this pathway because it does not assume full radical chain propogation (dashed blue arrow, Figure S3), and set a total CHOCHO yield from IEPOX oxidation at 28%.

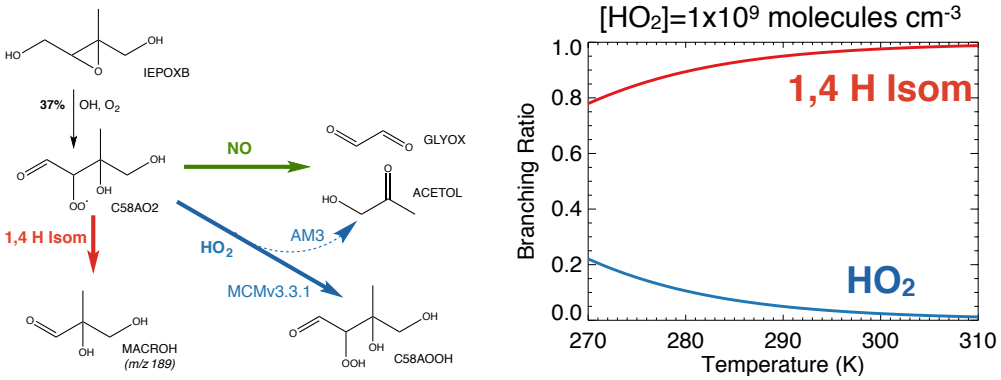

Figure S3: Left: Pathways of CHOCHO formation from the oxidation of IEPOX in MCMv3.3.1 [Jenkin et al., 2015]. Species are labeled with their names in MCMv3.3.1. The dashed blue arrow indicates the CHOCHO formation pathway from the reaction of the IEPOX peroxy radical (C58AO2) with HO_2 in AM3 [Li et al., 2016]. Right: Branching ratio between the reaction of the C58AO2 with HO_2 and isomerization, at a HO_2 concentration of 1×10^9 molecules cm^{-3}

However MCMv3.3.1 does not produce CHOCHO in high yield via this pathway as there is a competing (1,4) H-shift isomerization (red arrow, Figure S3), forming MACROH. The branching ratio as a function of temperature between HO_2 and the isomerization is shown in Figure S3 (right). This has been calculated with a HO_2 concentration of 1×10^9 molecules cm^{-3}. HO_2 concentrations simulated by GEOS-Chem over the Southeast US during SENEX were never above this concentration, so the plot in Figure S3 can be regarded as an upper limit for the HO_2 pathway. MCMv3.3.1 suggests that at 296K, HO_2 reactions with C58AO2 account for at most 3% of total loss.

The chamber experiments reported by Bates et al. [2014] also suggest that the majority of C58AO2 is lost via isomerization. The sum of products of the (1,4) H-shift isomerizations of IEPOXB peroxy radicals (including MACROH) were detected using chemical ionization mass spectrometry (CIMS), by monitoring the signal at $m/z = 189$. Bates et al. [2014] oxidized cis-IEPOXB under low-NO_x conditions and inferred yields of the $m/z = 189$ products that

were approximately 4 times higher than those formed via the HO_2 pathway (ACETOL and GLYC). Since ACETOL is a coproduced with CHOCHO, we set the yield of CHOCHO from IEPOX + HO_2 equal to the ACETOL yield derived from the low-NO_x cis-IEPOXB oxidation experiment (8.5%). The observed ACETOL yields cannot accomodate the 28% yield assumed in AM3, even when factoring in the reported 30% uncertainty in the measurements.

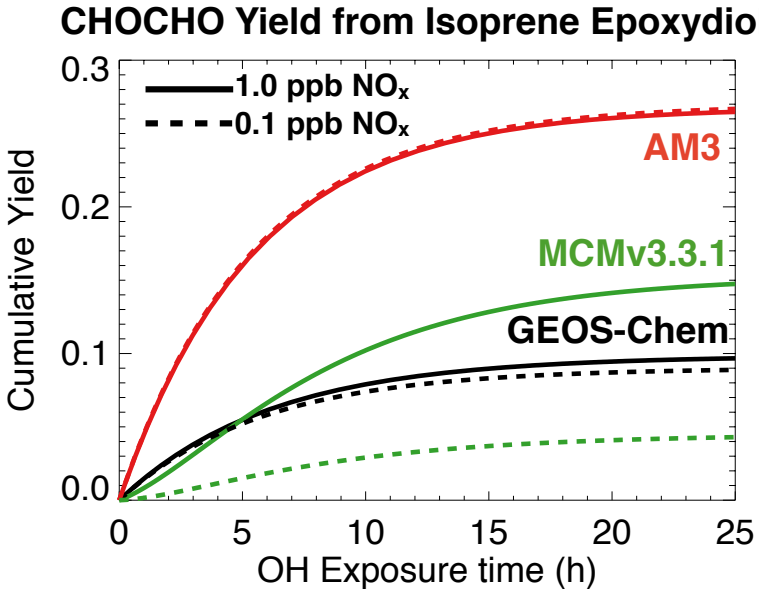

Figure S4: Cumulative time-dependent molar yields of CHOCHO from IEPOX oxidation in the GEOS-Chem, AM3 and MCMv3.3.1 chemical mechanisms. Results are from box model simulations described in the main text, calculated at two imposed NO_x concentrations (0.1 and 1 ppbv). The AM3 yield does not include contribution from GLYC oxidation. "OH exposure time" is equivalent to time for a constant [OH]=4×10^6 molecules cm^{-3}

Bates et al. [2014] also derived ACETOL yields from experiments involving the oxidation of cis- and trans-IEPOXB under high-NO_x ($\sim$ 570 ppb NO) conditions. At these NO levels, the (1,4) H-shift isomerization pathway should be minor. We combine the observed ACETOL yields with the measured yields of cis- and trans-IEPOXB and estimate a CHOCHO yield of 8.8% for the reaction of IEPOX+NO.

Figure S4 compares the cumulative CHOCHO yield from IEPOX in GEOS-Chem, MCMv3.3.1, and AM3, as a function of OH exposure time (Equation 3, main text). The GEOS-Chem yields are within the range simulated by MCMv3.3.1, however the NO_x-dependence of the yield is weaker. The yield realized by AM3 is approximately 2.5 times higher than GEOS-Chem after 25 hours of OH exposure time.

S3 Production of CHOCHO via isoprene peroxy radical isomerization

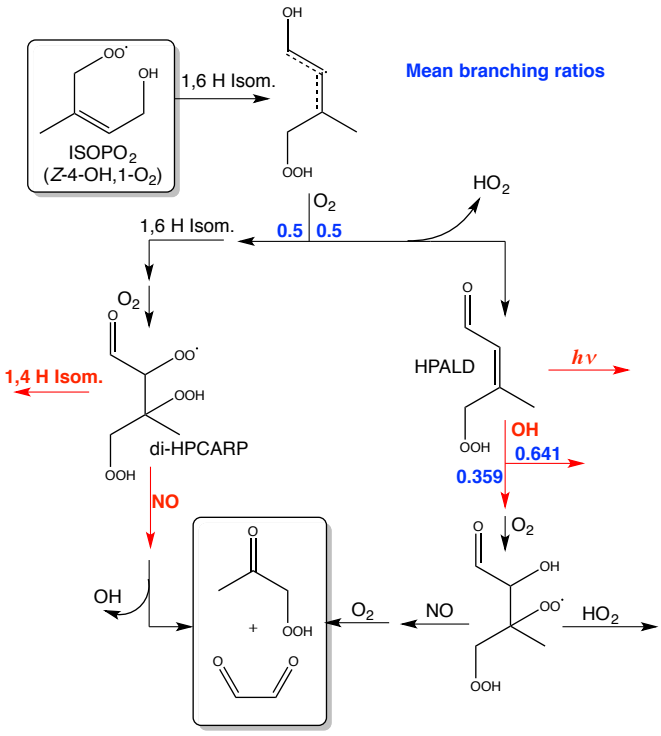

Figure S5: Main pathways to CHOCHO formation from the ISOPO2 isomerization in MCMv3.3.1 [Jenkin et al., 2015]. Only species relevant to CHOCHO formation are shown. Key reactions for determining the CHOCHO yield are highlighted in red.

.

Figure S5 shows the pathways to CHOCHO formation via ISOPO2 isomerization in MCMv3.3.1 [Jenkin et al., 2015]. ISOPO2 isomerization yields dihydroperoxy-formyl peroxy radicals (di-HPCARPs) in addition to HPALDs [Peeters et al., 2014]. In general, yields of CHOCHO via ISOPO2 isomerization in MCMv3.3.1 are negligable, as its formation via di-HPCARPs and HPALDs require NO. In contrast, CHOCHO production in AM3 is much stronger, as HPALD photolysis produces yields 25% CHOCHO. This yield is based on Stavrakou et al. [2010], however no mechanism for CHOCHO formation was provided. As such, we regard the MCMv3.3.1 protocol as more reliable. Nevertheless, analysis of the SENEX observations suggested that MCMv3.3.1 was missing a prompt source of CHOCHO under low-NOx conditions. This lead to our further examination of the MCMv3.3.1 $ISOPO_2$ pathways for missing reactions.

The (1,4) H-shift di-HPCARP isomerization was included in the MCMv3.3.1 protocol to be consistent with the updated chemistry of the methacrolein-derived α-formyl peroxy radical (MACRO2) [Crounse et al., 2012]. Chamber experiments suggest MACRO2 isomerization rates of ~ 0.5 s^{-1} [Crounse et al., 2012]. A (1,5) H-shift isomerization of the di-HPCARP

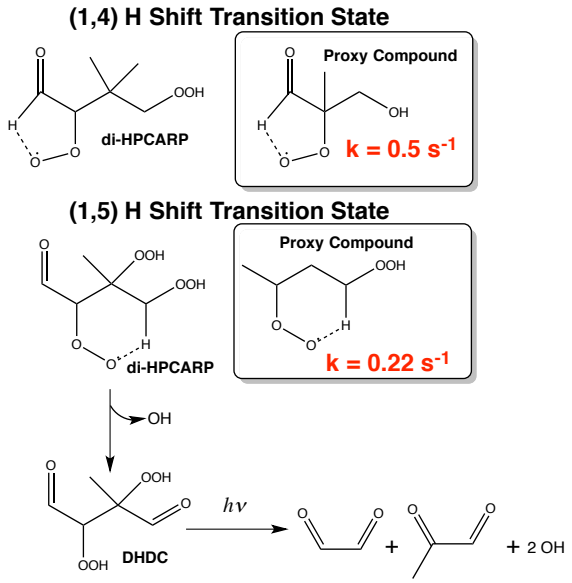

Figure S6: Transition states for the (1,4) and (1,5) H-shift isomerizations of the di-HPCARP leading to CHOCHO formation. These are compared to the proxy compounds used to determine their rates [Crounse et al., 2012, 2013]. The subsequent steps to CHOCHO formation from the (1,5) H-shift are also shown.

.

is also possible. Generally (1,5) H-shift isomerization rates are expected to be three orders of magnitude slower then the (1,4) H-shift. However recent work has shown that it can be strongly enhanced by the presence of functional groups with oxygen moities [Crounse et al., 2013], such as the terminal peroxide group in di-HPCARP. The closest structural proxy for the di-HPCARP from Crounse et al. [2013] ($CH_3CH(OO^{\cdot})CH_2CH(OOH)CH_3$, Figure S6) is predicted to have a isomerization rate of 0.22 s^{-1}, suggesting that the (1,5) H-shift isomerization of the di-HPCARP is competitive with the (1,4) H-shift. Here we include the di-HPCARP (1,5)H-shift in our revised mechanism, scaling the rate to 44% of the (1,4) H-shift, based on the ratio of the MACRO2 (1,4)H-shift and $CH_3CH(OO^{\cdot})CH_2CH(OOH)CH_3$ (1,5)H-shift rates.

The di-hydroperoxide dicarbonyl compound (DHDC) produced from the (1,5) H-shift isomerization can potentially lead to the production of CHOCHO via photolysis. Recent studies of the photolysis of HPALDs [Peeters et al., 2014], and carbonyl nitrates [Müller et al., 2014] have suggested mechanisms by which photon absorption on carbonyl chromophores can lead to dissociation of weaker bonds (e.g. O−OH) at near unity quantum yields. The same mechanisms are possible for DHDC. Assuming no interaction between the carbonyl chromophores, we estimate the cross section of DHDC to be twice the value of butenal, available from the 2006 IUPAC recommendations [Atkinson et al., 2006]. Combined with unity quantum yields, this yields a lifetime of $\sim$ 2.8 hours at midday. The actual photolysis rate may be faster than this estimate, as interactions between the peroxide and carbonyl groups may enhance the cross section analagous to the effect of nitrate groups adjacent to

carbonyl chromophores [Müller et al., 2014]. In the revised mechanism we set the DHDC photolysis rate equal to the HPALD photolysis rate. DHDC accounts for 26% of CHOCHO production from isoprene over the Southeast US in our simulations.

S4 Sensitivity to aerosol reactive uptake

Li et al. [2016] showed that CHOCHO concentrations are sensitive to aerosol reactive uptake. Although we only simulate CHOCHO loss to OH and photolysis, a reasonable estimate of the CHOCHO concentration with aerosol loss ($[CHOCHO]_a$) can be made assuming steady state;

$$[CHOCHO]_a = \frac{k_{OH}[OH] + J}{k_{aer} + k_{OH}[OH] + J}[CHOCHO] \tag{S1}$$

where $[CHOCHO]$, k_{aer}, k_{OH}, and J are the simulated concentration, aerosol loss rate to reactive uptake, OH reaction rate, and photolysis rate of CHOCHO respectively. k_{aer} is calculated following Jacob [2000];

$$k_{aer} = \left(\frac{a}{D_g} + \frac{4}{\nu\gamma}\right)^{-1} A \tag{S2}$$

a is the effective aerosol radius, D_g is the gas phase diffusion constant, ν is the mean molecular speed of CHOCHO, γ is the reactive uptake coefficient, and A is the aerosol surface area. We test the sensitivity with $\gamma = 2 \times 10^{-3}$ from Li et al. [2016].

Figure S7 shows the observed and simulated median vertical profiles of CHOCHO (with and without aerosol uptake) along the SENEX flight tracks. Inclusion of aerosol reactive decreases the median mixed layer (< 1 km) CHOCHO concentration by $\sim$ 10%. The difference between observed and simulated median mixed layer CHOCHO concentrations is -13% with the aerosol sink, comparable to that of HCHO (-14%).

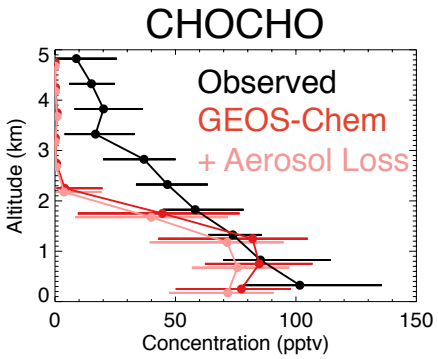

Figure S7: Median vertical profiles of CHOCHO concentrations during SENEX (June 1 - July 10 2013). Observed concentrations [Min et al., 2016] are compared to GEOS-Chem model values with and without aerosol uptake (Equation S1), sampled along the flight tracks. Horizontal bars indicate interquartile range. Altitudes are above ground level (AGL).

S5 Additional Supporting Figures

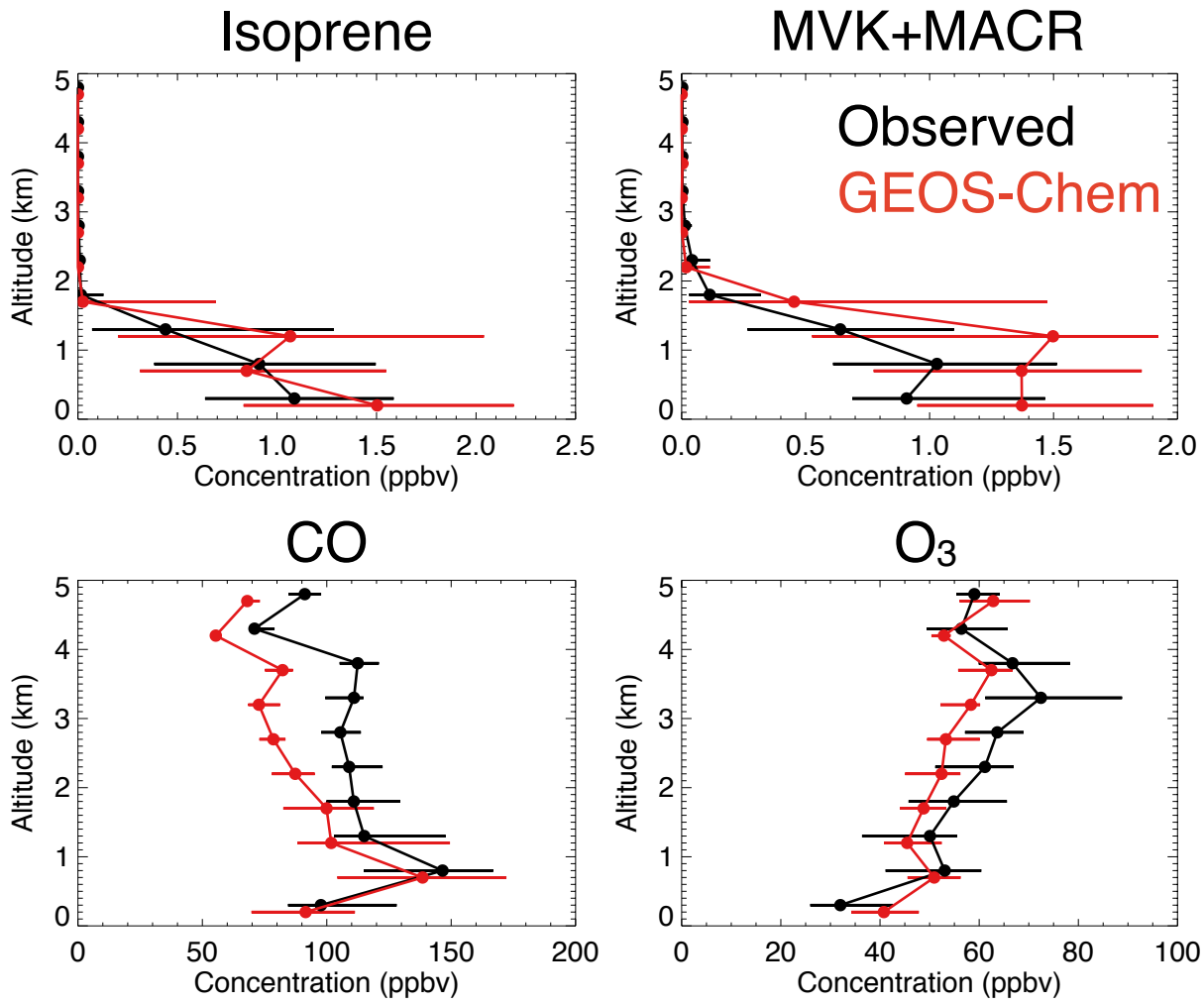

Figure S8: Median vertical profiles of isoprene, methylvinylketone+methacrolein (MVK+MACR), CO, and O_3 concentrations during SENEX (June 1 - July 10 2013). Observed concentrations are compared to GEOS-Chem model values sampled along the flight tracks. Horizontal bars indicate interquartile range. Altitudes are above ground level (AGL)

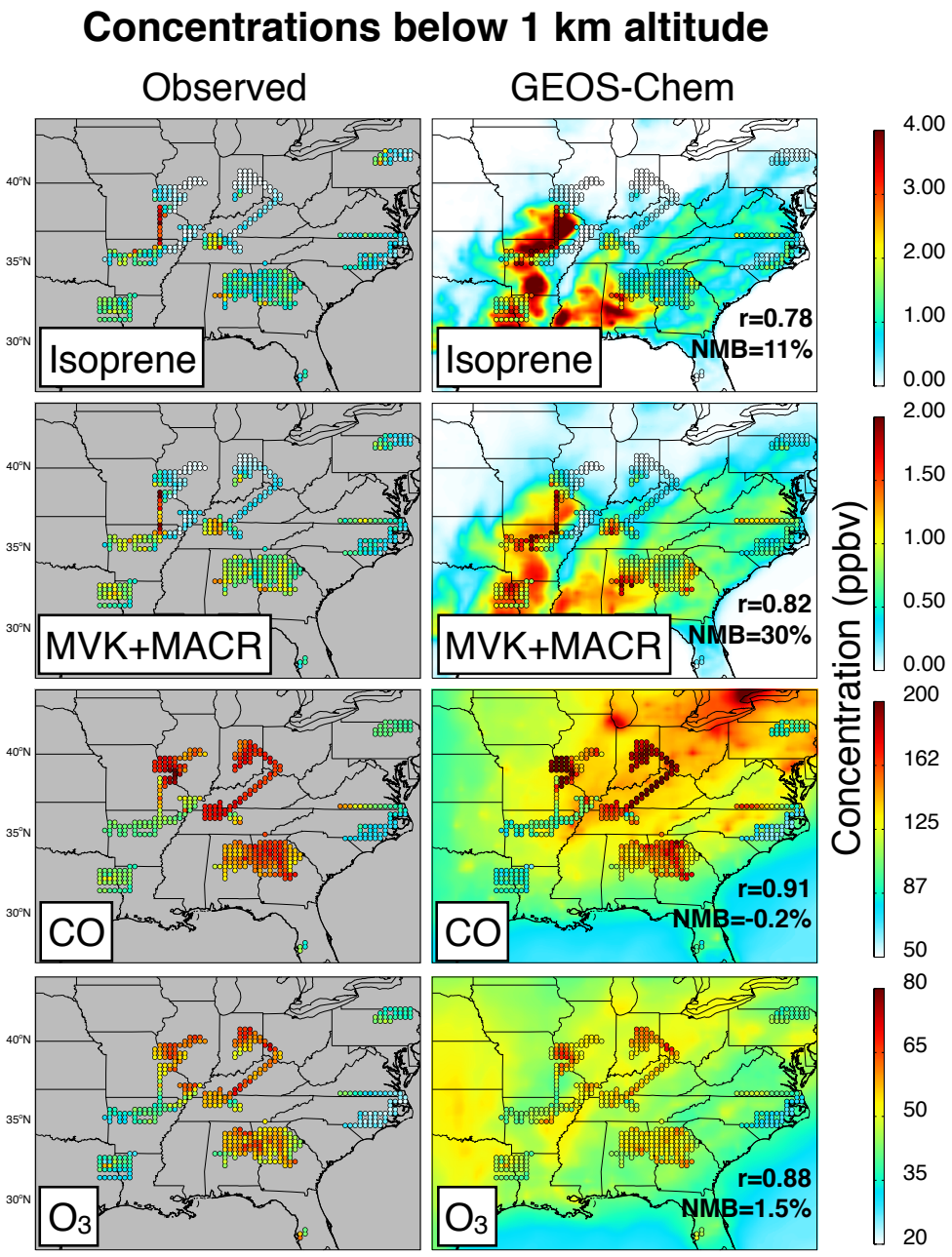

Figure S9: Isoprene, methylvinylketone+methacrolein (MVK+MACR), CO, and O_3 concentrations below 1 km AGL during SENEX (June 1 - July 10 2013). The grid squares show daytime aircraft observations compared to the colocated GEOS-Chem model values on the $0.25^{circ} \times 0.3125°$ model grid. Background contours in the right panels show the average model-simulated concentrations at 13 - 14 local time for the SENEX period. Comparison statistics between model and observation grid squares are shown as the correlation coefficient r and the normalized mean bias (NMB).

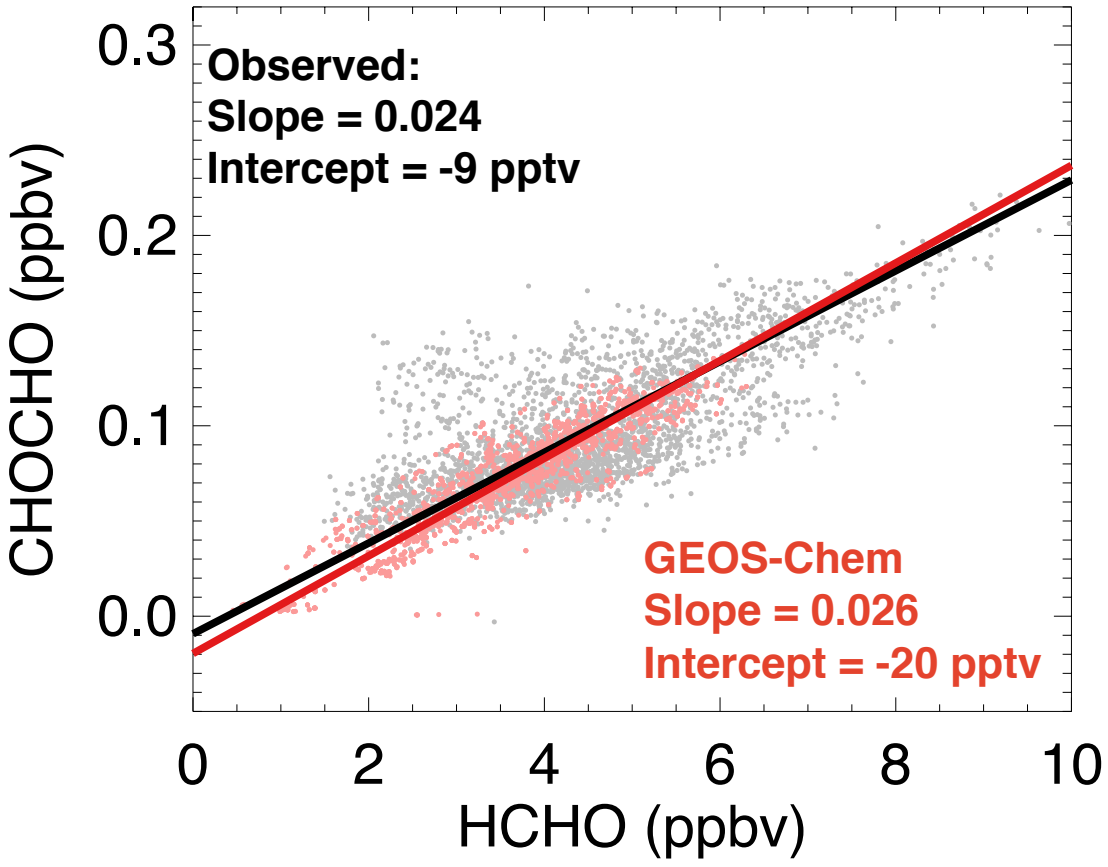

Figure S10: Relationship between CHOCHO and HCHO concentrations in the mixed layer (< 1 km AGL during SENEX (June 1 - July 10 2013). Observed values are compared to GEOS-Chem model values that have been rescaled to account for aerosol uptake (Equation S1). Lines and reported slopes are from reduced major axis regressions.

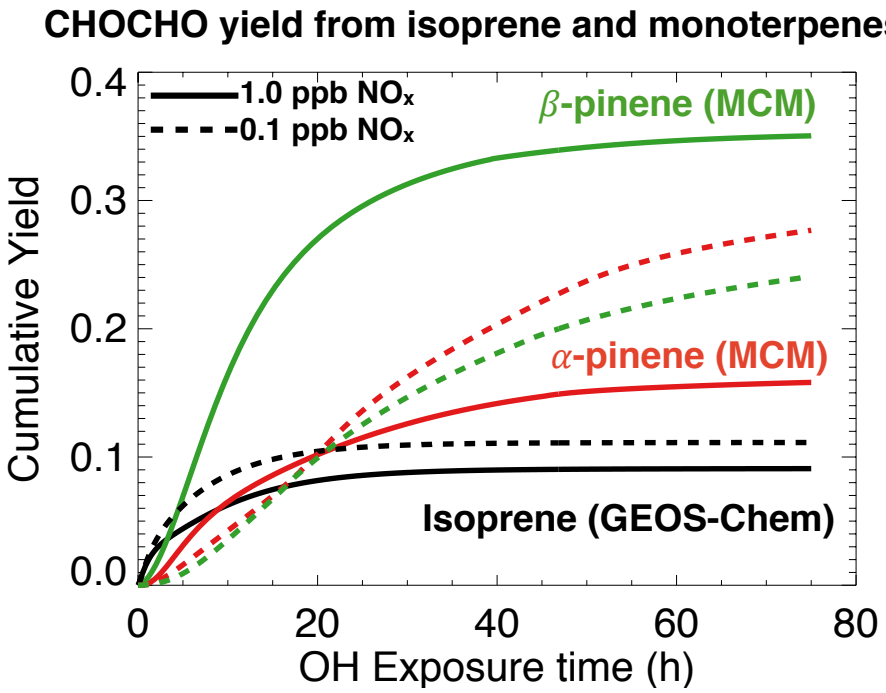

Figure S11: Cumulative time-dependent molar yields of CHOCHO from the oxidation of isoprene and monoterpenes. Results are from box model simulations described in the main text, calculated at two imposed NO_x concentrations (0.1 and 1 ppbv). The isoprene mechanism is from GEOS-Chem and the α-pinene and β-pinene mechanisms are from MCMv3.3.1. "OH exposure time" is equivalent to time for a constant [OH]=4×10^6 molecules cm^{-3}

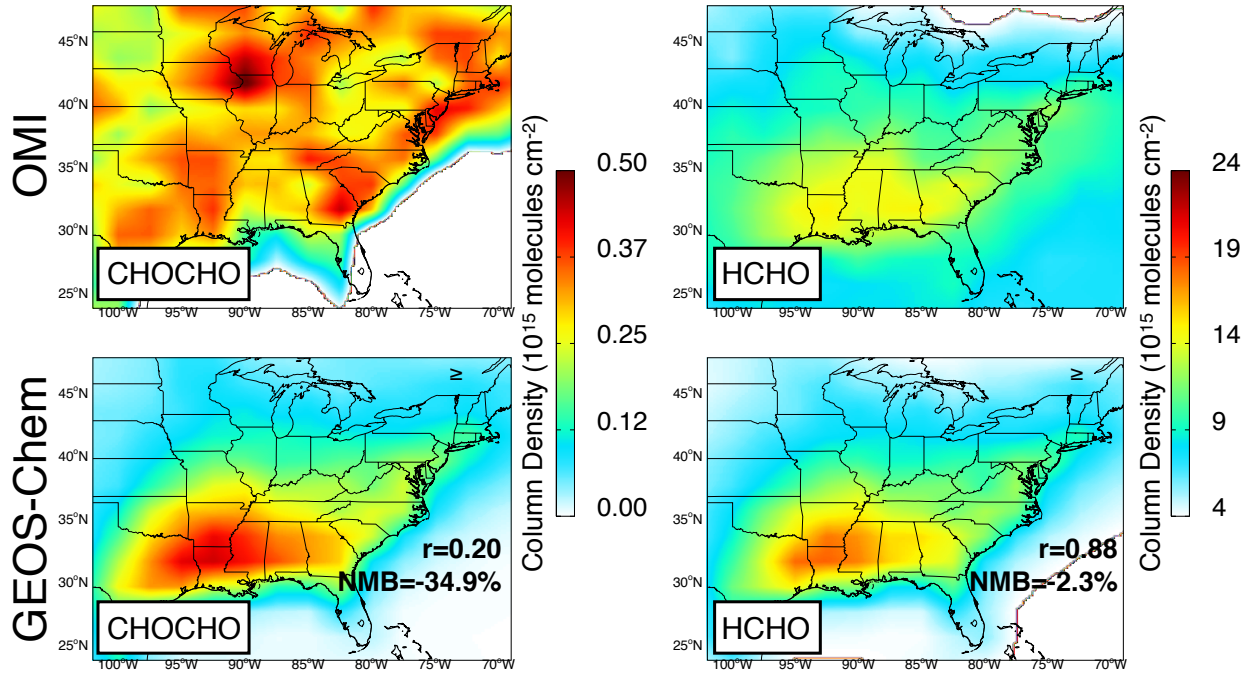

Figure S12: Mean CHOCHO and HCHO columns in summer (JJA) 2013. OMI satellite observations (top) are compared to GEOS-Chem model values (bottom). The OMI HCHO observations have been scaled up by a factor of 1.67 to correct for retrieval bias [Zhu et al., 2016]. The normalized mean bias (NMB) and spatial correlation (r) between GEOS-Chem and OMI in the eastern US ($75° - 100°$W, $29.5° - 45°$N) is shown within the GEOS-Chem panels.

References

R. Atkinson, D. L. Baulch, R. A. Cox, J. N. Crowley, R. F. Hampson, R. G. Hynes, M. E. Jenkin, M. J. Rossi, J. Troe, and IUPAC Subcommittee. Evaluated kinetic and photochemical data for atmospheric chemistry: Volume ii - gas phase reactions of organic species. *Atmospheric Chemistry and Physics*, 6(11):3625–4055, 2006. doi: 10.5194/acp-6-3625-2006. URL `http://www.atmos-chem-phys.net/6/3625/2006/`.

Kelvin H. Bates, John D. Crounse, Jason M. St. Clair, Nathan B. Bennett, Tran B. Nguyen, John H. Seinfeld, Brian M. Stoltz, and Paul O. Wennberg. Gas phase production and loss of isoprene epoxydiols. *The Journal of Physical Chemistry A*, 118(7):1237–1246, 2014. doi: 10.1021/jp4107958. URL `http://dx.doi.org/10.1021/jp4107958`. PMID: 24476509.

Nadezhda I. Butkovskaya, Nicolas Pouvesle, Alexandre Kukui, , and Georges Le Bras. Mechanism of the oh-initiated oxidation of glycolaldehyde over the temperature range 233-296 k. *The Journal of Physical Chemistry A*, 110(50):13492–13499, 2006. doi: 10.1021/jp064993k. URL `http://dx.doi.org/10.1021/jp064993k`. PMID: 17165875.

Arthur W. H. Chan, Melissa M. Galloway, Alan J. Kwan, Puneet S. Chhabra, Frank N. Keutsch, Paul O. Wennberg, Richard C. Flagan, and John H. Seinfeld. Photooxidation of 2-methyl-3-buten-2-ol (mbo) as a potential source of secondary organic aerosol. *Environmental Science & Technology*, 43(13):4647–4652, 2009. doi: 10.1021/es802560w. URL `http://dx.doi.org/10.1021/es802560w`. PMID: 19673246.

John D. Crounse, Hasse C. Knap, Kristian B. Ørnsø, Solvejg Jørgensen, Fabien Paulot, Henrik G. Kjaergaard, and Paul O. Wennberg. Atmospheric fate of methacrolein. 1. peroxy radical isomerization following addition of oh and o2. *The Journal of Physical Chemistry A*, 116(24):5756–5762, 2012. doi: 10.1021/jp211560u. URL `http://dx.doi.org/10.1021/jp211560u`. PMID: 22452246.

John D. Crounse, Lasse B. Nielsen, Solvejg Jørgensen, Henrik G. Kjaergaard, and Paul O. Wennberg. Autoxidation of organic compounds in the atmosphere. *The Journal of Physical Chemistry Letters*, 4(20):3513–3520, 2013. doi: 10.1021/jz4019207. URL `http://dx.doi.org/10.1021/jz4019207`.

J. A. Fisher, D. J. Jacob, K. R. Travis, P. S. Kim, E. A. Marais, C. Chan Miller, K. Yu, L. Zhu, R. M. Yantosca, M. P. Sulprizio, J. Mao, P. O. Wennberg, J. D. Crounse, A. P. Teng, T. B. Nguyen, J. M. St. Clair, R. C. Cohen, P. Romer, B. A. Nault, P. J. Wooldridge, J. L. Jimenez, P. Campuzano-Jost, D. A. Day, P. B. Shepson, F. Xiong, D. R. Blake, A. H. Goldstein, P. K. Misztal, T. F. Hanisco, G. M. Wolfe, T. B. Ryerson, A. Wisthaler, and T. Mikoviny. Organic nitrate chemistry and its implications for nitrogen budgets in an isoprene- and monoterpene-rich atmosphere: constraints from aircraft (seac4rs) and ground-based (soas) observations in the southeast us. *Atmospheric Chemistry and Physics Discussions*, 2016:1–38, 2016. doi: 10.5194/acp-2016-52. URL `http://www.atmos-chem-phys-discuss.net/acp-2016-52/`.

M. M. Galloway, A. J. Huisman, L. D. Yee, A. W. H. Chan, C. L. Loza, J. H. Seinfeld, and F. N. Keutsch. Yields of oxidized volatile organic compounds during the oh radical

initiated oxidation of isoprene, methyl vinyl ketone, and methacrolein under high-no$_x$ conditions. *Atmospheric Chemistry and Physics*, 11(21):10779–10790, 2011. doi: 10.5194/acp-11-10779-2011. URL http://www.atmos-chem-phys.net/11/10779/2011/.

Daniel J. Jacob. Heterogeneous chemistry and tropospheric ozone. *Atmospheric Environment*, 34(12–14):2131 – 2159, 2000. ISSN 1352-2310. doi: http://dx.doi.org/10.1016/S1352-2310(99)00462-8. URL http://www.sciencedirect.com/science/article/pii/S1352231099004628.

M. E. Jenkin, J. C. Young, and A. R. Rickard. The mcm v3.3.1 degradation scheme for isoprene. *Atmospheric Chemistry and Physics*, 15(20):11433–11459, 2015. doi: 10.5194/acp-15-11433-2015. URL http://www.atmos-chem-phys.net/15/11433/2015/.

Jingyi Li, Jingqiu Mao, Kyung-Eun Min, Rebecca A. Washenfelder, Steven S. Brown, Jennifer Kaiser, Frank N. Keutsch, Rainer Volkamer, Glenn M. Wolfe, Thomas F. Hanisco, Ilana B. Pollack, Thomas B. Ryerson, Martin Graus, Jessica B. Gilman, Brian M. Lerner, Carsten Warneke, Joost A. de Gouw, Ann M. Middlebrook, Jin Liao, André Welti, Barron H. Henderson, V. Faye McNeill, Samuel R. Hall, Kirk Ullmann, Leo J. Donner, Fabien Paulot, and Larry W. Horowitz. Observational constraints on glyoxal production from isoprene oxidation and its contribution to organic aerosol over the southeast united states. *Journal of Geophysical Research: Atmospheres*, 121(16):9849–9861, 2016. ISSN 2169-8996. doi: 10.1002/2016JD025331. URL http://dx.doi.org/10.1002/2016JD025331. 2016JD025331.

I. Magneron, A. Mellouki, G. Le Bras, G. K. Moortgat, A. Horowitz, and K. Wirtz. Photolysis and oh-initiated oxidation of glycolaldehyde under atmospheric conditions. *The Journal of Physical Chemistry A*, 109(20):4552–4561, 2005. doi: 10.1021/jp044346y. URL http://dx.doi.org/10.1021/jp044346y. PMID: 16833791.

Jingqiu Mao, Fabien Paulot, Daniel J. Jacob, Ronald C. Cohen, John D. Crounse, Paul O. Wennberg, Christoph A. Keller, Rynda C. Hudman, Michael P. Barkley, and Larry W. Horowitz. Ozone and organic nitrates over the eastern united states: Sensitivity to isoprene chemistry. *Journal of Geophysical Research: Atmospheres*, 118(19):11,256–11,268, 2013. ISSN 2169-8996. doi: 10.1002/jgrd.50817. URL http://dx.doi.org/10.1002/jgrd.50817.

K.-E. Min, R. A. Washenfelder, W. P. Dubé, A. O. Langford, P. M. Edwards, K. J. Zarzana, J. Stutz, K. Lu, F. Rohrer, Y. Zhang, and S. S. Brown. A broadband cavity enhanced absorption spectrometer for aircraft measurements of glyoxal, methylglyoxal, nitrous acid, nitrogen dioxide, and water vapor. *Atmospheric Measurement Techniques*, 9(2):423–440, 2016. doi: 10.5194/amt-9-423-2016. URL http://www.atmos-meas-tech.net/9/423/2016/.

J.-F. Müller, J. Peeters, and T. Stavrakou. Fast photolysis of carbonyl nitrates from isoprene. *Atmospheric Chemistry and Physics*, 14(5):2497–2508, 2014. doi: 10.5194/acp-14-2497-2014. URL http://www.atmos-chem-phys.net/14/2497/2014/.

Jozef Peeters, Jean-François Müller, Trissevgeni Stavrakou, and Vinh Son Nguyen. Hydroxyl radical recycling in isoprene oxidation driven by hydrogen bonding and hydrogen tunneling: The upgraded lim1 mechanism. *The Journal of Physical Chemistry A*, 118(38):8625–8643, 2014. doi: 10.1021/jp5033146. URL `http://dx.doi.org/10.1021/jp5033146`. PMID: 25010574.

T. Stavrakou, J. Peeters, and J.-F. Müller. Improved global modelling of ho_x recycling in isoprene oxidation: evaluation against the gabriel and intex-a aircraft campaign measurements. *Atmospheric Chemistry and Physics*, 10(20):9863–9878, 2010. doi: 10.5194/acp-10-9863-2010. URL `http://www.atmos-chem-phys.net/10/9863/2010/`.

L. Zhu, D. J. Jacob, P. S. Kim, J. A. Fisher, K. Yu, K. R. Travis, L. J. Mickley, R. M. Yantosca, M. P. Sulprizio, I. De Smedt, G. Gonzalez Abad, K. Chance, C. Li, R. Ferrare, A. Fried, J. W. Hair, T. F. Hanisco, D. Richter, A. J. Scarino, J. Walega, P. Weibring, and G. M. Wolfe. Observing atmospheric formaldehyde (hcho) from space: validation and intercomparison of six retrievals from four satellites (omi, gome2a, gome2b, omps) with seac 4 rs aircraft observations over the southeast us. *Atmospheric Chemistry and Physics Discussions*, 2016:1–24, 2016. doi: 10.5194/acp-2016-162. URL `http://www.atmos-chem-phys-discuss.net/acp-2016-162/`.